Foreword

Abstract

Atmospheric weapons tests, reactor accidents as well as reprocessing activities have contributed to global, regional and local contamination of artificial radionuclides in the environment during the last 60 years. Uranium as well as plutonium and other transuranics are of special concern due to their high radiotoxicity and long half-lives. There is still a lack of knowledge regarding ecosystem transfer, processes and mechanisms, which influences the predictive power of impact and risk models. The main purpose of this thesis was to obtain source term information on previous reprocessing activities. This was done by identifying radioactive particles, and by determining activity ratios and isotope ratios in sediment contaminated due to historical releases.

The investigated sediments were collected from sites downstream from selected reprocessing installations in the United States (Savannah River Site, Pond A) and the U.K. (Sellafield and Ravenglass). For comparison purposes two reference samples from Mayak PA (Reservoir 10 and Asanov Swamp), a comparable reprocessing installation in Russia, was included.

Radioactive particles (hot spots) were observed in the vertical profiles collected from both sites, in particularly from Sellafield using P imaging. Based on ESEM, U containing particles were identified. The distribution of activity concentrations for Cs, Am and Pu according to depth was obtained for the sediment cores provided from Savannah River Site and Sellafield using gamma-spectrometry, and alpha-spectrometry and ICP-mass spectrometry (^{238}Pu, ^{239}Pu and ^{240}Pu). This enabled calculations of the activity ratios (^{137}Cs/$^{239+240}$Pu, ^{241}Am/$^{239+240}$Pu and ^{238}Pu/$^{239+240}$Pu) and Pu isotopic ratios as a function of sediment depth. By comparing the results obtained, distinct signals different from the global fallout signal were seen for sediments from both sites.

The contamination from Savannah River Site can be characterized by a low ^{240}Pu/^{239}Pu isotope ratio and a high ^{137}Cs/$^{239+240}$Pu activity ratio compared to global fallout. Contamination from Sellafield can be characterized by a high ^{240}Pu/^{239}Pu isotope ratio and a high ^{241}Am/$^{239+240}$Pu activity ratio, and a low ^{137}Cs/$^{239+240}$Pu activity ratio compared to global fallout.

Historical changes in releases from SRS was also illustrated by changes in the Pu isotopic ratios, 0.11 ± 0.007 in the surface layer and 0.08 ± 0.007 in the deeper layer.

Compared to soil from Asanov Swamp (Mayak), Savannah River Site had similar ^{238}Pu/$^{239+240}$Pu activity ratio, but higher ^{240}Pu/^{239}Pu isotope ratios. Compared to sediment from

Reservoir 10 (Mayak), Savannah River Site had similar ^{240}Pu/^{239}Pu isotope ratio, but lower ^{238}Pu/$^{239+240}$Pu activity ratio. Sellafield (K2) had higher ^{240}Pu/^{239}Pu isotope ratio than both Savannah River Site and Mayak, but lower ^{238}Pu/$^{239+240}$Pu activity ratio than sediment from Reservoir 10 (Mayak). Thus, the combination of the ^{240}Pu/^{239}Pu isotope ratio and the ^{238}Pu/$^{239+240}$Pu activity ratio can be utilized to differentiate between source term, releases and contamination from the three sites.

Sammendrag

Atomprøvesprengninger, reaktorulykker og gjenvinning av brukt reaktorbrensel har bidratt til global, regional og lokal miljøforurensing av radioaktivt materiale i løpet av de siste 60 årene. Uran, samt plutonium og andre transuraner er av spesiell bekymring, på grunn av lange halveringstider og høy radiotoksisitet. Det er fremdeles mangel på kunnskap knyttet til overføringer, prosesser og mekanismer i økosystemet, noe som øker usikkerheten i konsekvens- og risikoanalyser.

Hovedhensikten med dette arbeidet var å innhente informasjon om kildeterm knyttet til tidligere reprosessering-aktiviteter. Det ble utført ved å identifisere radioaktive partikler, og ved å finne aktivitetsforhold og isotopforhold i sediment forurenset av historiske utslipp. Sedimentene ble samlet inn fra steder nedstrøms for utvalgte reprosesserings anlegg i U.S.A. (Savannah River Site, Pond A) og Storbritannia (Sellafield og Ravenglass). For sammenlikning ble det inkludert to referanseprøver fra Mayak PA (Reservoir 10 og Asanov Swamp), et sammenliknbart reprosesseringsanlegg i Russland.

Radioaktive partikler (hotspots) ble observert i den vertikale sediment-profilen for Savannah River Site, og spesielt for Sellafield (K2 og Ravenglass) ved hjelp av P imaging. Ved hjelp av ESEM ble uranpartikler identifisert. Dybdefordelingen av aktivitetskonsentrasjoner for Cs, Am og Pu ble innhentet ved hjelp av gammaspektrometri, og alfaspektrometri og ICP-massespektrometri (^{238}Pu, ^{239}Pu og ^{240}Pu). Det muliggjorde beregninger av aktivitetsforhold (^{137}Cs/$^{239+240}$Pu, ^{241}Am/$^{239+240}$Pu og ^{238}Pu/$^{239+240}$Pu) og Pu isotopforhold som funksjon av dybde i sediment. Ved å sammenlikne resultatene ble det observert signaler forskjellig fra globalt nedfall for sediment fra begge stedene.

Forurensningen fra Savannah River Site kan kjennetegnes ved en lav ^{240}Pu/^{239}Pu isotoprate og en høy ^{137}Cs/$^{239+240}$Pu aktivitetsrate, sammenliknet med globalt nedfall. Forurensningen fra Sellafield kan kjennetegnes ved en høy ^{240}Pu/^{239}Pu isotoprate og en høy ^{241}Am/$^{239+240}$Pu aktivitetsrate, samt en lav ^{137}Cs/$^{239+240}$Pu aktivitetsrate sammenliknet med globalt nedfall.

Historiske endringer i utslipp ble observert for Savannah River Site, illustrert av endringer i Pu isotop rater, 0.11 i øvre lag og 0.08 i nedre lag.

Sammenliknet med jordprøven fra Asanov Swamp (Mayak) hadde Savannah River Site sammenliknbar $^{238}Pu/^{239+240}Pu$ aktivitetsrate, men høyere $^{240}Pu/^{239}Pu$ isotoprate. Sammenliknet med sediment fra Reservoir 10 (Mayak) hadde Savannah River Site sammenliknbar $^{240}Pu/^{239}Pu$ isotoprate, men lavere $^{238}Pu/^{239+240}Pu$ aktivitetsrate. Sellafield hadde høyere $^{240}Pu/^{239}Pu$ isotoprate enn både Savannah og Mayak, men lavere $^{238}Pu/^{239+240}Pu$ aktivitetsrate enn sediment fra Reservoir 10 (Mayak). Det er dermed mulig å skille mellom kildeterm, utslipp og forurensning fra de 3 stedene.

Table of Content

1. Introduction

Radioactive elements, both natural and artificial, are present in the environment. Radionuclides are unstable, i.e. the composition of protons and neutrons in the nucleus will change over time until a stable state is attained. Simultaneously with the n-p or p-n transformations in the core, ionizing radiation such as alpha (He nuclides), beta (electrons or positrons) or gamma radiation is emitted. The daughter nuclide can also be radioactive, and the process continues until stability is reached. Key sources of naturally occurring radionuclides (NORM) include cosmic rays (tritium, C-14), K-40 and U or Th containing bedrocks. Artificially produced radionuclides originate from manmade processes and technology such as medicine, nuclear weapons and nuclear power production.

Artificial radionuclides have been introduced to the environment since the start of the nuclear era. The most significant sources are associated with the nuclear weapon and fuel cycles: the nuclear weapons tests (atmospheric, underground and underwater), the nuclear fuel cycle (including mining, milling, fuel fabrication, reprocessing and waste management), and accidents involving nuclear installations, detonation of nuclear weapons, accidents with nuclear driven satellites, airplanes, and submarines (IAEA 2011). The nuclear weapons tests, conducted between 1945 and 1980, caused global fallout of radionuclides into the environment, and it is estimated that 3500 kg plutonium were distributed globally (IAEA 2011).

Reprocessing plants were originally a major source of environmental contamination, when discharges went directly into rivers or into the sea during normal operation. Nuclear reprocessing plants have contributed to discharges of uranium, as well as plutonium and other transuranics into the environment, which are of special concern due to their long half-lives and high radiotoxicity. Sellafield discharges have for instance contributed to marine contamination of radionuclides spreading far distances into the arctic environment. In contrast, most of the releases from Mayak PA, Russia, is still contained in Lake Karachay and reservoirs.

Radionuclide exposure raises concern about potential harm to humans and other living organisms. In risk assessments, hazard, dose and effects need to be characterized. Following deposit, the ecosystem transfer and radionuclide behavior in the environment affects the exposure, uptake and short- and long-term impact and risk. Transfer and transport depend on the source and release scenario as well as on the speciation of radionuclides deposited in the environment and on transformation processes (interaction, particle weathering), changing the

speciation over time (Salbu et al. 2004; Salbu 2009). The bioavailability depends on the physico-chemical form of radionuclides (e.g. size, structure, morphology, oxidation states and charge properties) (Salbu 2000).

Many sources can affect the same territories, and it is most useful to identify sources of contamination. The composition of the contamination such as element ratio, isotope or atom ratio can be utilized to differentiate between sources. Detailed knowledge on previous deposition can also be utilized to obtain information about environmental transport and transfer mechanisms to improve the knowledge base needed in environmental impact and risk assessments.

Source term provides information on the release characteristics, which depend on the magnitude of the event, composition, physical and chemical form, and mode of radionuclides released during reactor operation, accident or detonation (Gaidar 2011). Characterizing radioactive particles is usually ignored in source terms, but should be included as particles can carry substantial radioactivity. Radioactive particles have been released into the environment as a consequence of nuclear weapons tests and the nuclear fuel cycle operations. However, the recognition of their importance have earlier been overlooked. They behave differently from simple ions or molecules in the environment with respect to transport and bioavailability, give rise to inhomogeneous distributions, and may act as a long term point source.

This thesis focuses on historical releases from reprocessing activities and the contamination of downstream sediments. By comparing signals based on activity ratios (Cs, Am and Pu) as well as Pu isotope ratios in sediments at 3 different sites (U.S., U.K., and Russia), differences and similarities in the source terms and releases are investigated

This thesis includes: section two that provides historical background of the selected sites and site specific information necessary to provide insight related to the selected samples, some relevant theory background, as well as the objectives and hypothesis of the project. Section three that provides the methodology and describes the experimental work performed. The results are presented and discussed in section 4, while the concluding remarks are to find in section 5.

1. Background

Scientific progress throughout the 18th century led to an increased understanding of the nature of atoms, and these discoveries would later lead to the development of nuclear weapons. The Manhattan Project, a research project led by the Unites States assisted by the United Kingdom and Canada, successfully developed the world's first nuclear weapon, and executed the first atmospheric nuclear test in Alamogordo in 1945. Approximately three weeks later, the American detonation of nuclear weapons on the two Japanese cities Hiroshima and Nagasaki ended the Second World War, but began a nuclear weapons race and the Cold War between the United States and the Soviet Union. The detonation of the atomic bombs demonstrated the great political influence that possessing weapons of mass destruction could have, and the Soviet Union did not wish for U.S. or its allies to influence the Eastern European region. And so, the nuclear weapons race began.

The situation of political and military tension that arose between the Eastern and Western blocs led to a fierce rearmament with massive nuclear production and atmospheric test detonations. The USSR was in a hurry to develop their own nuclear weapons, which they managed to do in secrecy. They detonated their first atomic bomb in 1949, whereas the U.K.'s first weapons test occurred in 1952 (Tvedt & Tjelmeland 2014). Each nuclear program was highly classified. However, despite all efforts, classified information was obtained by espionage. Especially remarkable is that the USSR was able to develop and detonate an atomic bomb in only a few years (1945-1949). The U.S. nuclear arsenal became their front line of defense until 1964, when President Johnson called for a reduction in the production of nuclear material. The introduction of the non-proliferation agreement in 1967, led to an agreement that prevented the spread of nuclear weapons. This resulted in a change in operation towards civilian purposes and reduced the atmospheric detonations.

The discovery of fission energy led to the development of the atomic bomb. Here, energy is released when a uranium or plutonium atom undergoes nuclear fission, approximately 200 MeV for both ^{235}U and ^{239}Pu (Lilley 2013). A critical mass of ^{235}U or ^{239}Pu will cause an uncontrolled nuclear chain reaction resulting in an explosion. This explosion releases heat, radiation and fission products. Fissionable material is produced from fertile material through neutron bombardment, and reprocessing technology is necessary to enable chemical separation of fissionable ^{239}Pu and ^{235}U from irradiated nuclear fuel. Reprocessing activities involve the

collection and storage of irradiated fuel from reactors, dissolution of the fuel, and solvent extraction to separate plutonium, uranium and fission products (Webb et al. 2006).

1.1. Nuclear reactors and reprocessing power plants

Los Alamos produced the plutonium used in the first nuclear weapons, through the Manhattan project. Another of the first U.S. nuclear installations was Hanford Site, Washington. Both sites used graphite-moderated reactors. The USSR decided to start their own weapons program after the Second World War, and Mayak Production Association (Mayak PA) was established.

By 1948, their first uranium-graphite reactor commenced operation, and by August 1949 plutonium was separated and converted into high-purity metallic plutonium components (Christensen et al. 1997).The USSR managed to test their first nuclear weapon that same year. Major expansion of the site followed, as five more nuclear reactors were built between 1949 and 1955 (Christensen et al. 1997). When the USSR had managed to develop their own nuclear weapon, the U.S. construction of the Savannah River Site (SRS) had as purpose to produce as much weapons-grade material as possible, through focusing on improvements in design to optimize production. This effort was to assure that the U.S. did not fall behind the Soviet Union. The U.S. and the U.K. were allies, however, the U.K decided to develop their own nuclear weapons, and started building their own installation at Windscale.

Early discharges at SRS and Mayak PA were released directly into nearby streams and rivers, causing contamination of whole river systems. Concerns about the environmental impact of such practices later led to the construction of reservoirs. At Mayak PA, reservoir 10, the first of the two largest industrial reservoirs, was constructed in 1956 (Skipperud 2004). At SRS the first seepage basin system, connected to R-reactor, was in use from 1958 (Carlton et al. 1994). At Sellafield, discharges were released directly to the Irish Sea from 1952, with a peak in the 1970s (Vintró et al. 2000).

Reprocessing technology applies for both military and civil production. The military purpose was to produce ^{239}Pu from irradiated ^{238}U fuel, and chemically separate it to weapons-grade plutonium. Later, civil reprocessing took over, where fissile U and Pu are recovered to become new fuel as either enriched fuel (^{235}U) or MOX-fuel (Pu), for energy and research purposes. This change in operations involved a difference in production methods, where the fuel was

irradiated for a longer period of time (increased burn-up times). ^{240}Pu is produced when ^{239}Pu absorbs a neutron rather than undergoing fission, and is difficult to separate from ^{239}Pu. The decreased need for ^{239}Pu enabled longer irradiation times for the uranium fuel, which caused a higher fraction of ^{240}Pu in the products.

1.1.1. Savannah River Site, U.S.

The Savannah River Site (SRS) is a nuclear installation built in the early 1950s, by the U.S. Department of Energy (USDOE). It is located in the state of South Carolina, U.S. Its original purpose was to produce radioactive material for use in nuclear weapons. The site consisted of five production reactors (C, K, P, L, R), a heavy water production facility, a fuel and target fabrication facility and two chemical reprocessing plants (F, H) (Hinton & Pinder III 2001). The nuclear power reactors produced radioactive material such as ^{239}Pu and tritium. Between 1953-1955, the reactors became operational, although they were shut down periodically for maintenance, safety upgrades, and replacement of fuel and targets (U.S.E.P.A. 2012).

All SRS reactors were pressurized heavy-water reactors. Heavy water (D$_2$O) was used as moderator and primary coolant (Lilley 2013), and uranium fuel was inserted into aluminum clad rods (Hinton & Pinder III 2001). Heavy water as moderator allows for natural uranium as fuel (99.3 % ^{238}U and 0.7% ^{235}U). The primary product of operation was ^{239}Pu. A change in operations occurred in the 1970s, to produce ^{238}Pu for NASA's space exploration program (heat-source and electricity). The recovery of plutonium from irradiated target and spent fuel elements happened in two chemical separation facilities (F-area and H-area). The last SRS reactor shut down in 1988. Since then, non-defense related activities such as the building of a MOX-facility and other industrial, medical and research projects has continued in addition to extensive environmental clean-up programs.

The R-reactor was the first production reactor at SRS, in operation from 1953. Its purpose was to produce plutonium. The secondary cooling system consisted of river water, as a once-through cooling. This could receive fission products and fuel elements from leakage in the primary cooling system in the reactor. Heated and radioactive discharges were released directly into the stream channel that was subsequently flooded by Pond C and the Hot Arm of Par, to Joyce Branch which was a tributary of the Lower Three Runs Creek (pers. comm. John Pinder). The reactor later used recycled water from an artificial pond system as a secondary cooling system.

The purpose of the artificial pond system was to capture contaminated soil to protect the water quality of nearby rivers from reactor discharges.

In 1958, R-reactor started discharging cooling water to Pond C, and pumping started from C back to R-reactor (pers. comm. John Pinder). To accommodate the heat and radiation releases from R, the discharge canal was extended northward beyond the stream course to Pond C into what became Pond A. Pond A received thermal discharges from September 1961 (Whicker et al. 1990). The discharges continued through the R-canal to Pond B and subsequently into the North Arm of Par Pond (*Fig. 1)*. Whereas the discharges to the Pond C area had previously occurred from the canal, there remained a diversion box that would allow the discharges to flow into Pond C. This control structure was designed to shunt water out of the canal system in the case of flooding (pers. comm. John Pinder). R-reactor closed down in June 1964, and R-canal was no longer in use.
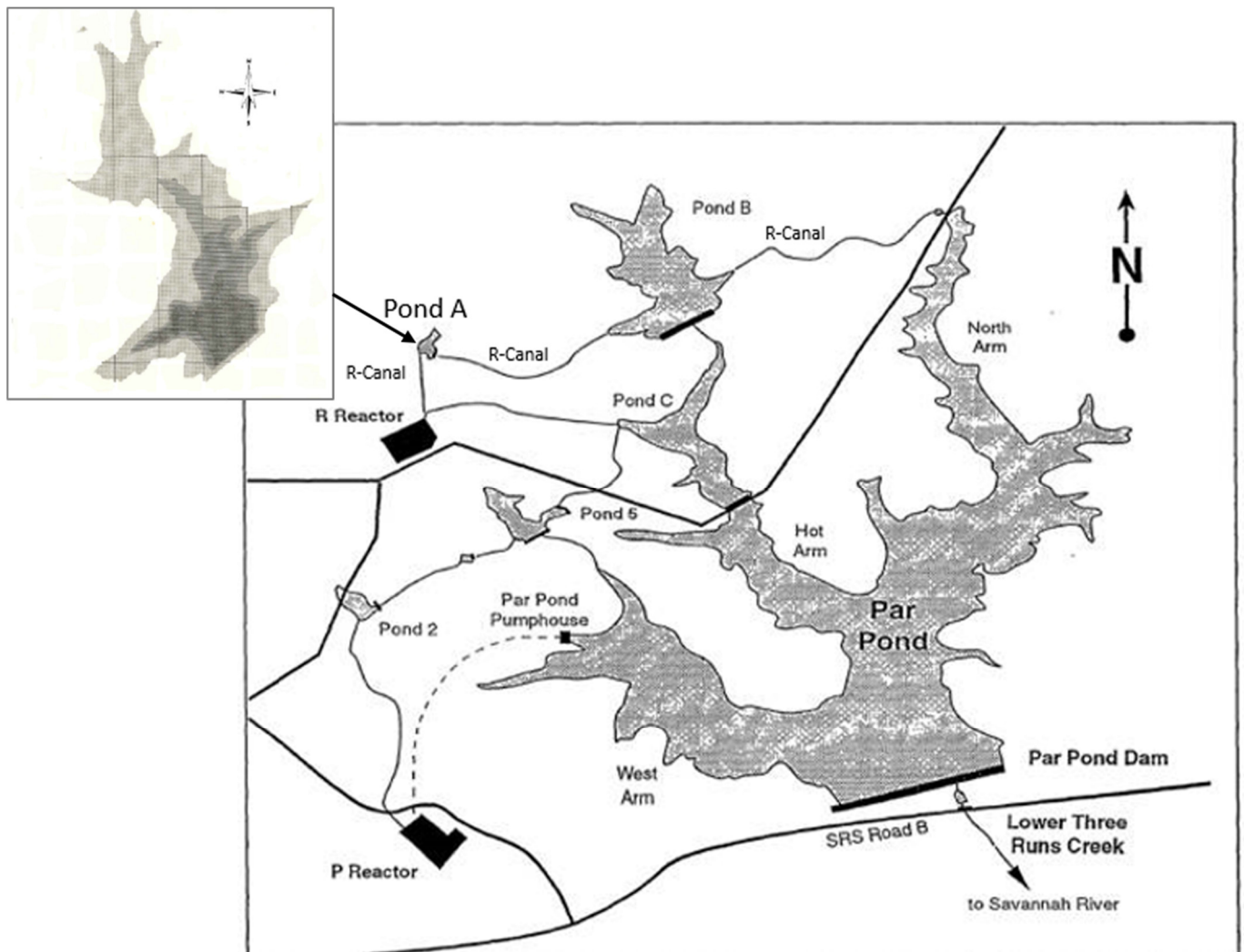
Figure 1. Par Pond cooling water system (Halverson 1998). Map Pond A (courtesy of T. Hinton.).

Pond A (*Fig. 2*) is a shallow (mean depth ~ 0.5 m), small pond (size ~ 0.05 km^2), located north of R- reactor, approximately 0.8 km down R-canal (Abraham et al. 2000). The pond contains a high density of aquatic vegetation and undecomposed tree material. When R-reactor was in operation, water flow was 11 m^3/s, which raised the water level to approximately 1 m (Abraham et al. 2000). Watermarks on the concrete walls indicates that the water level at times reached even higher (pers. comm. John Pinder). The mean residence time has been estimated to approximately 1h, which limited the sorption and transfer to sediments. Roughly 1-2% of the released radionuclides may have been sorbed to Pond A sediments during the one hour residence time (Abraham et al. 2000). Pond A received discharges from September 1961 to June 1964.

Figure 2. Pond A, Savannah River site (Photo: O. C. Lind).

Chemical separation processes caused the greatest atmospheric and aquatic releases of plutonium into the environment at SRS. The majority of atmospheric releases occurred in 1955 and 1969, caused by exhaust filter failure. The majority of aquatic releases caused contamination within sedimentation basins, but considerable uncertainty exists in estimates of plutonium releases to the site streams, particularly prior to the 1970s when the few measurements made were on gross alpha activity (Hinton & Pinder III 2001) .

The earliest discharges were poorly documented, which influences available information about discharges from R-reactor. Primary sources of contamination to Pond A were leakage from spent fuel rods in storage basins (Abraham et al. 2000). The R-area releases mostly resulted from abnormal operating events such as fuel failure and faulty storage containment, which caused long lasting releases. The most significant release into the environment occurred in the early years of operation, when activation products and fission products were released to seepage basins and site streams. One event in 1957 was caused by a failure of a fuel tube in the R-area isolation basin. In 1964 the maximum release at the site occurred, due to a failed fuel tube stored in a leaking containment (Carlton et al. 1994).

Table 1 shows an overview of documented discharges to SRS. The table includes discharges from R-reactor and the separation facilities F and H. These are the facilities with the most extensive release history, and are the most relevant for the case provided in this work. Discharge data from the separation facilities are from startup to 1988 and 1989 for F and H seepage basins, respectively (Carlton et al. 1994). The lack of documentation makes estimations of radionuclide discharges to Pond A difficult, but a rough estimate is possible to obtain by looking at the total discharges from R-reactor between 1953 and 1964. Pond A was in operation for three years, and the damming of PAR Pond happened in 1958. Assuming the releases were evenly distributed during the reactors life time, the yearly discharge to the seepage basins would be approximately 2 GBq plutonium and 55 TBq cesium. Assuming that 1 -2% sorbed to the Pond A sediments would give an inventory of maximum 120 MBq of plutonium and 3 TBq of cesium during the three years that the pond received discharges from R-reactor. Discharges were released in pulses, but it is not possible to estimate the fraction received by Pond A, hence, the numbers are not trustworthy.

Table 1 (Carlton et al. 1994; Hinton & Pinder III 2001)

Facility		Years in operation	Radionuclide	To streams	To seepage basins	To atmosphere
Reactor	R	1953-1964	Cesium	8 TBq	333 TBq	unknown
			Plutonium	$\geq$ 0.4 GBq	11 GBq	unknown
Separation facilities	F	1954-2002	Cesium	minimal	8 TBq	22 GBq
			Plutonium	9 GBq	267 GBq	91 GBq
	H	1955 - present	Cesium	minimal	7 TBq	0.1 TBq
			Plutonium	10 GBq	161 GBq	47 GBq

1.1.2. Sellafield, U.K.

Sellafield, formerly known as Windscale and Calder Works (until 1981), is a nuclear reprocessing site located on the coast of the Irish Sea, in Cumbria, England (*Fig. 3*). The site covers an area of approximately 4 km^2. Construction of the nuclear facility started in 1947 and included two nuclear reactors and a reprocessing plant. Its purpose was to produce plutonium for weapon production. The two reactors, called the Windscale Piles, was air-cooled and graphite-moderated. In the 1950s, four Magnox reactors (known as Calder Hall) started nuclear power generation for civil purposes. Low-level radioactive waste have been released into the North-Eastern Irish Sea since beginning of operations in 1952, in both planned discharges and accidental events.

Figure 3. Sellafield site (http://suppliers.sellafieldsites.com/procurement-opportunities/).

Reprocessing activity at Sellafield (Windscale) has contributed to radioactive discharges to the Irish Sea since the beginning of operations in 1952. Throughout the period 1952-2000, approximately 610 TBq of $^{239+240}$Pu was discharged, and sediments of the Western Irish Sea are now estimated to contain 20 TBq of ^{239,240}Pu (Remotrans 2004). Low level liquid wastes were routinely discharged into the eastern basin of the Irish Sea by a pipe-line extending 2.5 km into the sea, ending 20 m below the water surface (Pentreath 1985).

The major source of contamination in the early 1950s was the processing of nuclear fuel for production of nuclear weapons. However, since the late 1950s, production has switched to the reprocessing of fuel for commercial purposes such as energy production (Vintró et al. 2000). ^{239,240}Pu discharges are well documented(Gray et al. 1995), and peaked during the early- to mid-1970s (*Fig. 4)*. Some releases were chronic and authorized, while others were unplanned events.
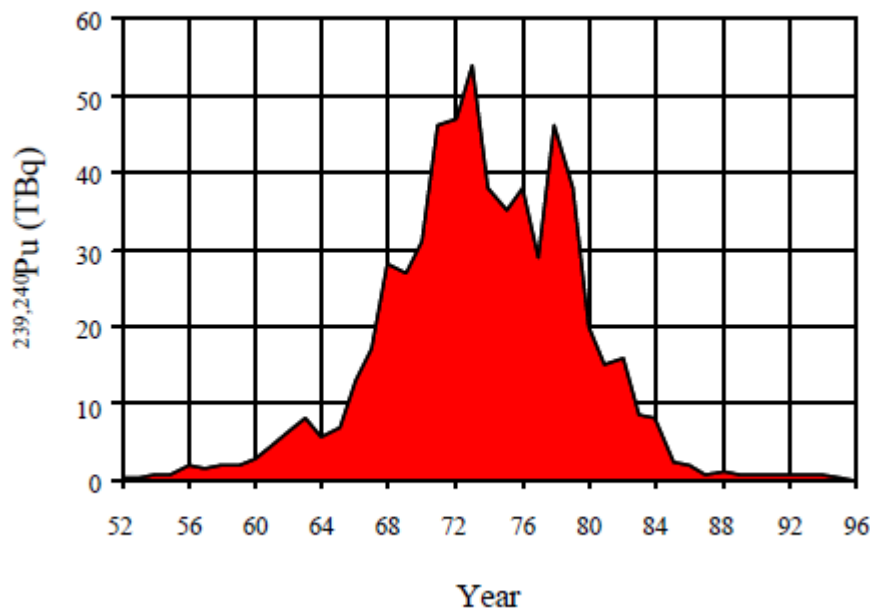
Figure 4. Historical discharges of $^{239,\ 240}$Pu Sellafield (Vintró et al. 2000).

The two most important chronic releases from Sellafield are: 1) discharges of plutonium to the atmosphere and to the Irish Sea during the 1950s-1960s; and 2) atmospheric releases of irradiated uranium oxide particulates from the Windscale Piles in the mid-1950s (Webb et al. 2006). The chronic release of uranium fuel oxide as particulates occurred due to ruptured fuel cartridges at Windscale Piles.

In the period 1950-2000, numerous unplanned operational events occurred at Windscale, in addition to authorized discharges. This led to atmospheric discharges of plutonium, summarized by Webb et al. (2006). One was the Windscale fire, a reactor fire at Windscale Pile no. 1 between the 10th and 11th of October in 1957(Gray et al. 1995). The graphite moderator caught fire due to the release of Wigner energy (Wakeford 2007). When graphite is bombarded with neutrons the crystal lattice of carbon is altered and the potential energy of the graphite increases. An attempt to release the energy under control, by heating and cooling the graphite, led to a fire in the core. The subsequent release of radioactive material is known as the worst accidental discharge in the U.K.

Transuranic inventory stored in sediment presents a long-term risk of remobilization. Discharges of cesium and plutonium from Sellafield into the Irish Sea have been incorporated into sediments, and is now a potential source of radioactive contamination. Exposure may happen by resuspension or redissolution of sediment (Cook et al. 1997). Mixing of surface sediment by tidal currents and wave activity results in mixing of radioactivity in upper layers (Kershaw et al. 1999). The sub-tidal, muddy sediments are not subjected to very strong tidal currents, but do undergo extensive mixing due to bioturbation, e.g. mixing by benthic organisms (Kershaw et al. 1999). The sub-tidal sediments in the vicinity of the discharges, along the Cumbrian coast and in the Western Irish Sea contain the highest concentrations of radioactivity in the surface sediments. There is evidence of remobilization of Sellafield derived radionuclides (Morris et al. 2000), causing contamination to be detected along the Norwegian coast (IAEA 2011).

1.2. Theory

Information regarding radionuclide nature and chemistry, particle characteristics, and isotope and activity composition are necessary to characterize the source term. Source term characteristics include isotopic and activity ratios, activity concentrations and physic-chemical forms. They are essential to determine inventories, ecosystem transfer mechanisms, transport in the environment, and to perform environmental impact assessments.

1.2.1. Radionuclide chemistry

Cesium

Cesium exists both naturally and artificially. It has about 40 known isotopes. The most known are the stable ^{133}Cs, the short-lived ^{134}Cs (2.062 y) and the long-lived ^{135}Cs ($2.6*10^6$ y), in addition to ^{137}Cs (30.17 y). Manmade sources are nuclear reactor operations and nuclear weapons tests. Any presence of ^{134}Cs in the environment indicates recent contaminations, while ^{137}Cs is still present in the environment after atmospheric tests and the Chernobyl accident. ^{137}Cs is produced by fission of irradiated nuclear fuel (e.g. ^{235}U) (Carlton et al. 1994), and disintegrates by β^-decay (0.5120 MeV, 94.6%) and subsequent gamma emission (0.662 MeV) to ^{137}Ba.

Uranium

Uranium is in the actinide group, with atomic nr 92. Uranium is present in the environment both naturally and due to human activities. Naturally occurring uranium mainly consists of ^{235}U (0.72%), ^{238}U (99.27%) and trace levels of ^{234}U. It occurs in two main oxidation states in nature: the reduced, immobile state U(IV), or the oxidized, more soluble and mobile state, U(VI). Relevant isotopes for this study are ^{235}U and ^{238}U. ^{235}U has a half-life of $7.04*10^8$ y, is fissile, and is used as energy source for nuclear weapons and power production. ^{238}U has a half-life of $4.47 * 10^9$ years, alpha-decays (4.198 MeV) through two short-lived daughters to ^{234}U, and continues down the uranium decay series ending as lead (Vandenhove et al. 2010). ^{238}U can also be fertile, absorbing a neutron and resulting in the production of ^{239}Pu.

Plutonium

Plutonium is the second transuranium element, discovered in 1940 by irradiation of uranium by deteurons followed by β-decay of ^{238}Np. Small energetic differences between oxidation states enables the presence of Pu to exist in four oxidation states simultaneously. Plutonium form large, highly charged and reactive cations, and has generally low solubility and low mobility. Generally, the lower oxidation states, Pu(III) and PU(IV), are more stable under acid conditions, while Pu(VI) is stable at high pH, and Pu(V) is most stable in neutral pH conditions(Neu et al. 2011). Plutonium is predominantly of anthropogenic origin, but it also occurs naturally due to neutron capture in naturally occurring uranium.

Plutonium isotopes are produced in nuclear reactors by irradiating uranium fuel with slow neutrons. The relevant isotopes for this study are ^{238}Pu, ^{239}Pu, ^{240}Pu and ^{242}Pu (*table 2*) .^{238}Pu has been used for thermoelectric power in spacecraft missions, 1 kg =22 mill kWh heat (Vandenhove et al. 2010).

The most common isotopes of plutonium emit high-energy alpha particles with energies around 5 MeV. Most of them have very long half-lives, and are of special concern. Relevant isotopes, their half-lives, main decay modes and radiation energy, in addition to their production methods are listed in *table 2*.

Carbonate complexes of Pu are of major interest because of the presence of carbonate (organic material) in natural waters and the high affinity of Pu ions to bond strongly with carbonate.

Humic substances affects the oxidation states of Pu, by reduction of higher oxidation states to more stable Pu(IV) (Neu et al. 2011). When Pu(IV) is above trace level and particulate matter is present, solids or suspended colloids become predominant form.

Table 2. Relevant isotopes of plutonium and their main decay mode, half-life, radiation energy and production method (Neu et al. 2011).

Isotope	Half-life	Decay mode	Radiation energy (MeV)	Method of production
^{238}Pu	87.7 years	α	5.499 (70.9%)	^{242}Cm daughter
^{239}Pu	2.411×10^4 years	α	5.157 (70.77%)	^{239}Np daughter
^{240}Pu	6.561×10^3 years	α	5.168 (72.8%)	multiple n-capture
^{242}Pu	3.7×10^5 years	α	4.902 (76.49%)	multiple n-capture

Americium

All americium isotopes are highly toxic, and are hazardous to humans if ingested or inhaled. Relevant isotopes for this study are ^{241}Am, ^{243}Am and ^{244}Am. The trivalent oxidation state is the most stable under environmental conditions. ^{241}Am is a decay product of ^{241}Pu. It has a half-life of 432.7 years, and alpha-decays with E_α = 5.486 MeV (86%), and gamma-decays with energy 0.059 MeV (35.7%) (Runde 2011).

$$^{239}Pu\,(n,\gamma)^{240}Pu(n,\gamma)^{241}Pu(\beta^-) \rightarrow\, ^{241}Am$$
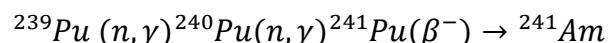
1.2.2. Radioactive particles

"Radioactive particles are defined as localized aggregation of radioactive atoms that give rise to inhomogenous distribution of radionuclides significantly different from that of the matrix background" (IAEA 2011). Aquatic particles are defined as ≤ 45 µm diameter, and radioactive species with size ranging from $0.001 \mu m - 0.45$ µm are referred to as colloids or pseudo-colloids (*Fig. 5*). Particle bound radionuclides behaves differently compared to ions, molecules or complexes. Low molecular mass species are mobile and bioavailable, while colloids and particles are assumed to settle in sediment.
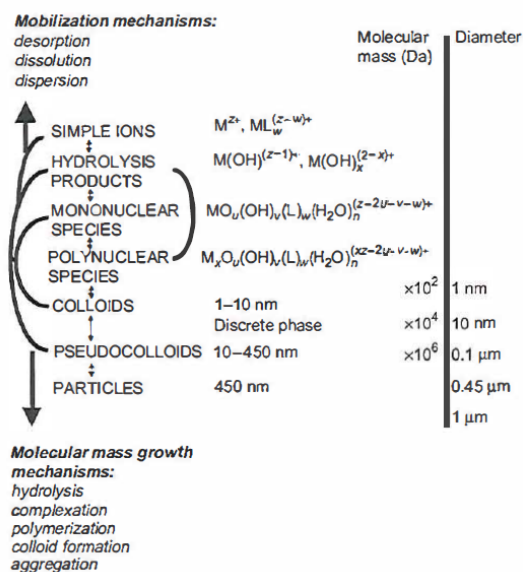
Mobilization mechanisms:
desorption
dissolution
dispersion

		Molecular mass (Da)	Diameter
SIMPLE IONS	M^{z+}, $ML_w^{(z-w)+}$		
HYDROLYSIS PRODUCTS	$M(OH)^{(z-1)+}$, $M(OH)_x^{(z-x)+}$		
MONONUCLEAR SPECIES	$MO_u(OH)_v(L)_w(H_2O)_n^{(z-2u-v-w)+}$		
POLYNUCLEAR SPECIES	$M_xO_u(OH)_v(L)_w(H_2O)_n^{(xz-2u-v-w)+}$		
COLLOIDS	1–10 nm Discrete phase	$\times10^2$ $\times10^4$	1 nm 10 nm
PSEUDOCOLLOIDS	10–450 nm	$\times10^6$	0.1 μm
PARTICLES	450 nm		0.45 μm 1 μm

Molecular mass growth mechanisms:
hydrolysis
complexation
polymerization
colloid formation
aggregation

Figure 5. Size classes of radionuclides in the marine environment (Salbu 2000).

The importance of considering radioactive particles

Measurements of environmental radioactivity are often based on the assumption of homogenously distributed radioactivity. However, radioactive particles can be present in the environment due to nuclear weapons tests or nuclear accidents, and effluents leaked from reprocessing plants during routine operation are also believed to contain a large fraction of non-reactive radioactive particles and colloids (Salbu 2000). Assumptions of homogenous distribution can therefore lead to overestimations of inventory.

Ignoring the presence of radioactive particles may also lead to errors in estimating risk to human health and when assessing long-term ecological consequences. Radioactive particles in sediment may act as a long-term diffuse source, caused by weathering (decomposition of particle and release of radionuclides). Weathering rates depend on particle composition, structural changes, and chemical conditions such as pH and redox (Salbu & Krekling 1998). In less contaminated areas, a significant source of transuranic contamination is from remobilization of contaminated soils and sediments (Oughton et al. 2000). This illustrates the importance of assessing long term behavior of sediment inventory. Uptake of radioactive particles can accumulate in the body and cause local internal dose, and direct contact can cause burns etc. Some studies have shown that radioactive particles can be retained in mussels and snails, causing radiation damage (IAEA 2011; Jaeschke et al. 2014).

A large amount of work have been done to improve understanding of the implications on transport and dispersion of radioactive particles. The Irish Sea sediment samples have earlier been proven to contain U fuel particles (Jernström 2006; Lind 2006), and the presence of these particles is a bigger problem than earlier believed. Monitoring programs have identified radioactive particles at public beaches adjacent to Sellafield, assumed to have entered the marine environment in the vicinity of the old effluent pipeline (Sellafield Ltd. 2014). Beach monitoring in 2013-14 identified 109 particles, and of them, 101 was alpha emitters. The findings reflect an underlying trend for particles to move onshore with subsequent alongshore transport.

Radioactive particles are generally expected to be transported in a way reflecting their size and density (fine-grained particles as silt and coarser grained particles as sand) (Sellafield Ltd. 2014). The Sellafield offshore mud patch is a stable area of fine silts, and the littoral zone consists of coarser sandy silt. The number of particles and their distribution on the seabed is unknown, but it is assumed that a significant offshore population of fine coarsed radioactive particles remain. Such particles may move northward by currents towards The Cumbrian coastal mud patch where they would preferentially be deposited, based on elevated activity concentrations in the zone.

1.2.3. Source determination

Sources of radioactive contamination can be determined by evaluation of isotopic composition and activity composition, as activity and isotopic ratios vary according to source and release scenario. The ratios relevant for this study are the $^{240}Pu/^{239}Pu$ isotopic ratio, and the activity ratios $^{238}Pu/^{239+240}Pu$, $^{241}Am/^{239+240}Pu$ and $^{137}Cs/^{239+240}Pu$. The global fallout activity ratio for $^{241}Am/^{239+240}Pu$ is 0.36 (Zheng et al. 2012), and for $^{137}Cs/^{239+240}Pu$ it is ranging between 28 and 37 (Sakaguchi et al. 2009).

The $^{240}Pu/^{239}Pu$ atomic ratio provides information about fuel burn-up and can reveal weapon design and the scale of explosion from nuclear weapons tests (Lee & Clark 2005). Combining $^{240}Pu/^{239}Pu$ ratio with $^{238}Pu/^{239+240}Pu$ activity ratios can separate sources that otherwise could be difficult, such as the separation between global fallout and weapons grade Pu, or the separation between Pu powered reactors and civil reactor waste (*Fig. 6*).
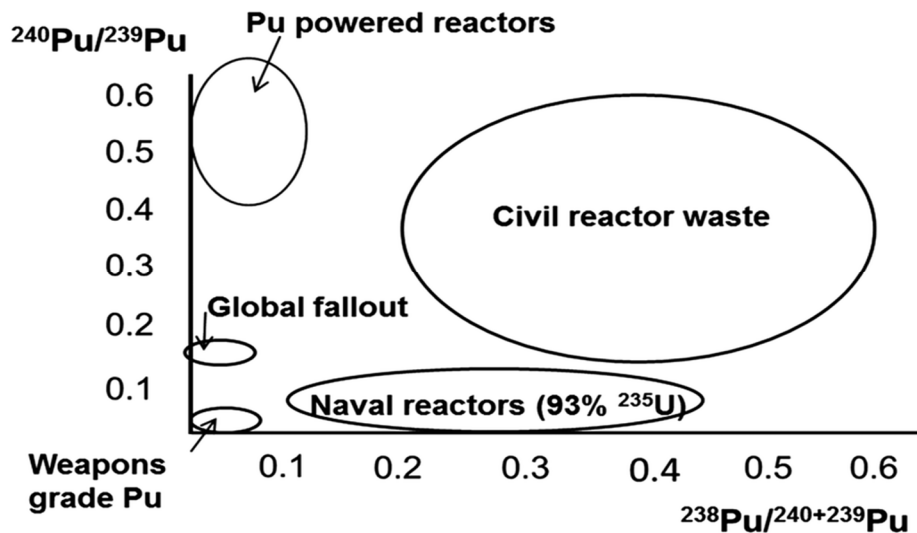
Figure 6. Pu ratios and source determination (Cagno et al. 2014; Skipperud 2004).

The average $^{240}Pu/^{239}Pu$ isotopic ratio from global fallout is 0.18, and the global fallout $^{238}Pu/^{239+240}Pu$ activity ratio is ~0.03. (Buesseler 1997). Comparing some ratios from Sellafield, Hanford, Mayak and Hanford illustrates the variation between low burn-up sources (*table 3*).

Table 3. Comparison of ratios from different sites compared to global fallout.

Source	$^{240}Pu/^{239}Pu$ isotopic ratio	$^{238}Pu/^{239+240}Pu$ atomic ratio	Reference
Global fallout	0.17-0.19	0.03	(Buesseler 1997)
Weapons production	0.01-0.07		(Nassef et al. 2008)
Power reactors	0.23-0.67		(Nassef et al. 2008)
Sellafield		0.4-0.18	(Remotrans 2004)
SRS (low burn up)	0.062		(Dai et al. 2002)
Hanford (low burn-up)	≤0.04		(Dai et al. 2005)
Mayak (low burn up)	≤0.06	≤0.04	(Skipperud 2004)

1.3. Objectives and hypotheses

The overall objectives of the present work is to obtain source term information on previous reprocessing activities by

- identification of radioactive particles

- determining activity ratios for cesium, americium and plutonium

- determining isotope ratios for plutonium

in sediment contaminated due to historical releases from the Savannah River Site (U.S.) and Sellafield (U.K.). For comparison purposes, two reference samples from reservoir 10 and Asanov Swamp, Mayak PA (Russia) are included. Sources of contamination and potential changes in operation will be identified by the help of a new method for Pu analysis, using a new type of ICP-MS instrument.

The project hypotheses are as follows:

1. The radionuclide composition in contaminated sediments will vary with depth, reflecting the historical changes in nuclear production operation.
2. Contamination originating from the different reprocessing plants will have significantly different plutonium ratios, providing a fingerprint for both installation and operational modes. This will distinguish between historical discharges from the different reprocessing plants in the U.S, U.K., and Russia.
3. The release of refractory radionuclides suggests release of radioactive particles, and identification of heterogeneous distribution and radioactive particles should be possible.

2. Materials & Methods

2.1. Sample description

In this study archived sediment samples originating from Pond A, Savannah River Site (SRS), U.S., and the Eastern Irish Sea, Sellafield, U.K., were provided. Some uncertainty exists as to sampling time for SRS and release time for Sellafield, so the results are not decay corrected but presented in this thesis with reference date 01.01.2015.

The samples from SRS were collected in Pond A (33°28'N, -81°58' W), by the Savannah River Ecology Laboratory (SREL). The samples were made available to NMBU as a courtesy of Tom Hinton (SREL), during an NMBU fieldtrip to SRS in 2008. The sample population consisted of 22 sediment cores of varying depth (maximum depth 24 cm), which had been divided into 1 cm increments and dried before storage.

The Sellafield samples consisted of a sediment core from the sub tidal offshore sediment as well as an intertidal surface sediment sample. The samples originated from a collaborative expedition, DIAPLU, to the eastern Irish Sea and to intertidal areas of the Cumbrian coast in July 2002, and they were made available to NMBU, as a courtesy of P. Kershaw, CEFAS and D. Boust, IRSN. The sediment core SUB-112 (K2) was collected from the Irish Sea sub-tidal sediments (SUB-112; 54° 23.85'N, -3°, 34.99'W(Gouzy 2004)), and the intertidal sediment sample was collected from the intertidal reaches of the Esk Estuary, Ravenglass (INT-010; 54° 20.35'N, -03° 24.09'W) (*Fig. 7)*. The sub-tidal sediment core was retrieved using a flucha box-corer, and it was sealed and frozen whole before shipment to Norway. The core was subsequently sliced and unfreezed before being refrozen the same year (pers. comm. Ole Lind). The sediment core provided was 30 cm deep and divided into 9 increments (ranging from 0-2 cm, 2-4 cm, 4-6 cm, 6-8 cm, 8-10 cm, 10-15 cm, 15-20 cm, 20-25 cm, and 25-30 cm). The intertidal sediment sample was dried at room temperature and dry sieved (Remotrans 2004).
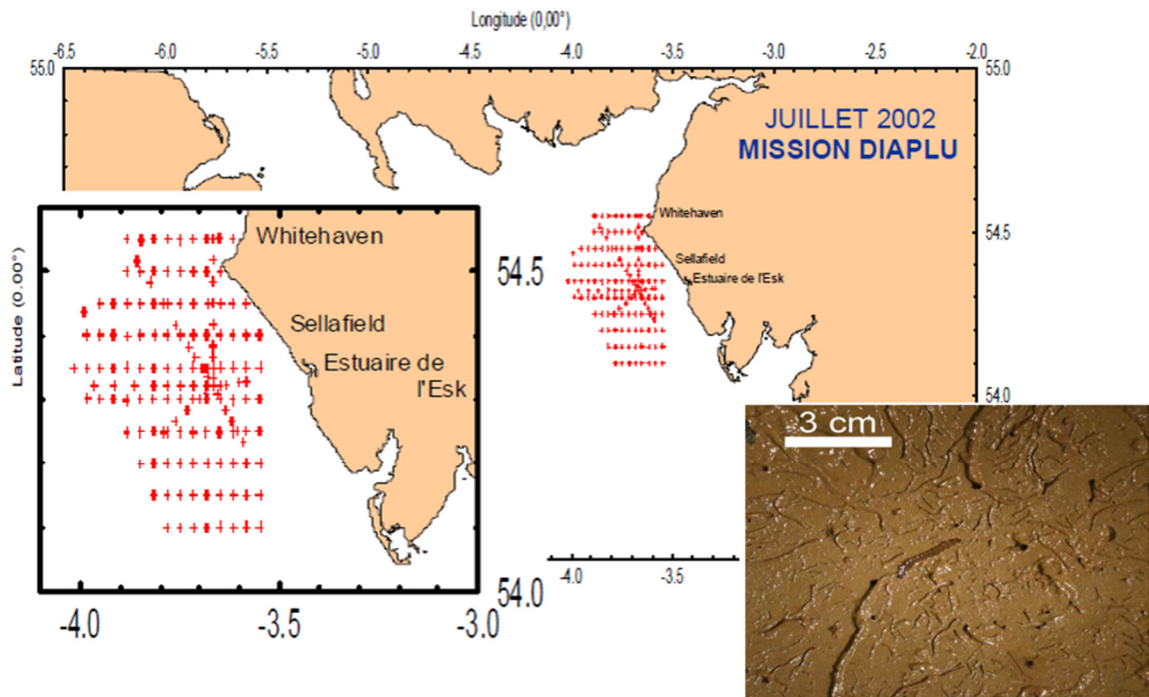
Figure 7. Sample locations DIAPLU collaboration 2002, and Esk Estuary surface sediment (Gouzy 2004),

For comparison and quality assurance purposes, two in-house standards originating from Mayak PA were included. Mayak 2626 sediment was collected from reservoir 10, and Mayak 3516 soil from Asanov Swamp.

2.2.   Sample preparation

Sample preparation includes all steps necessary to prepare the samples for measurements. Two different approaches for sample preparation were included, as both bulk sample- and particle-analyses were performed. The bulk sample population consisted of sediment cores A9 (SRS) and K2 (Sellafield) in addition to selected reference material for quality assurance. Particle samples consisted of selected samples from both sediment cores (SRS and Sellafield K2) in addition to the surface sediment sample from Ravenglass.

2.2.1. Particle samples

Sample preparation for particle samples consisted of mounting sediment onto paper before subjection to autoradiography. Sediment samples were mounted in three different ways: mounted onto contact-paper and covered by a thin plastic film; distributed loosely on paper and covered by a plastic film; and mounted by thin layers onto glue strips and exposed directly to the plate.

2.2.2. Bulk samples

Pretreatment, pre-concentration and chemical separation was necessary before measuring plutonium due to complex sample matrices, low concentrations of plutonium nuclides, their varying oxidation states, and the need for complete purification from other actinides to avoid interference of overlapping alpha-energies and masses (L'Annunziata 2012). The addition of a yield determinant, with different alpha energies and mass of the analytes, enabled monitoring of losses in the procedure as well as obtaining the original concentrations of analytes. Analytical blanks assured that potential contamination was kept as low as possible, in addition to providing procedural detection limits. All chemicals introduced in the preparation and separation processes were of PA (pro-analysis) quality.

Pre-treatment and radiochemical separation of Pu

^{242}Pu was chosen as the yield determinant, on the assumption of the same chemical and physical behavior to other Pu isotopes. ~24 pg ^{242}Pu tracer was weighed and added to aliquots of sediment (0.3g-5g). 15 ml concentrated HNO$_3$ was added before samples were digested in an ultraclave (UltraClave 3, Milestone Ltd.). High pressure (200 bar) in the closed vessel allowed high temperatures (260 ℃) by micro waves to be achieved, allowed efficient digestion of sample and prevented boiling. After digestion, the samples were filtrated through 125 mm glass microfiber filters. The extract was evaporated to dryness before plutonium was separated from the bulk matrix.

Pu-isotopes had to be separated from other actinides present in the bulk material. Ion exchange and extraction chromatography are suitable choices for soil and sediment samples, and ion exchange Ag 1x8 was selected for the current work.

Anion exchange was performed as described by Clacher (1995). The samples were taken up in 25 ml of 8M HNO_3. Fe(II)sulfate was added and heated gently to reduce all Pu to Pu(III). After cooling, 1 ml of 15 % $NaNO_2$ was added and heated, to evaporate nitrous gasses and to oxidize Pu to Pu(IV). The samples were cooled down in maximum 30 minutes and subsequently added to 2ml columns prepared with Ag 1x8 anion resin. The columns were pretreated with 20 ml of 2M $NaNO_3$ followed by 50 ml of 8M HNO_3. 50 ml of 8M HNO_3, and then 40 ml of 9M HCl was added, before plutonium was eluted as $PuCl_4$ by adding 40 ml solution of 1 ml 50% HI in 100 ml of 9M HCl. The Pu-fraction was contained in acid-washed beakers, and evaporated to dryness. 3x2 ml concentrated HNO_3 was added to assure removal of iodine. The samples were then evaporated to dryness. The Pu fraction was dissolved in 10 ml of 5 % HNO_3 with 0.2 % HF before introducing the sample to ICP-MS.

Selected samples from ICP-MS measurements were subsequently prepared for alpha spectrometry, by evaporating to dryness, before adding 2 ml of concentrated HNO_3. 8 ml of 5% $NaSO_4$ (sodium hydrogen sulphate) was added just before dryness. The solution was evaporated to dryness before dissolution in 6 ml of destilled water, before electro deposition onto stainless steel plates. The electro-deposit cell was filled with 15 ml 15% Na_2SO_4 (sodium sulphate) and 0.26M $(NH_4)_2C_2O_4H_2O$ (ammonium oxalate) as well as adding the sample (6 ml) and rinsing the beaker (6ml destilled H_2O). Electrodeposition of plutonium onto stainless steel disks was performed by applying a voltage (10 V) and current (0.4 A) for 2.5 h. Before turning off the power supply, 1 ml of 4M KOH was added to the cell to prevent redissolution of Pu. The disk was rinsed with MQ-water and ethanol, before fixating the deposition by heating on a heat-plate at 80℃ for 2 minutes. After cooling, the disks were placed in alpha spectrometers for counting.

LOI – Loss On Ignition

Aliquots of the samples from SRS and Sellafield (K2) were ashed in a Carbolite CWF120 furnace to determine Loss On Ignition (LOI). 1g sub samples were weighed directly into 50 ml glass beakers before being dried overnight at 105℃, to determine residual moisture. The samples were subsequently ashed at 550 ℃ overnight, before the LOI was determined.

$$\% \text{ LOI} = \frac{\text{weight of dry sample} - \text{weight of sample after ignition}}{\text{weight of dry sample}} * 100$$

Moist content was found to be less than 1 % for most samples, with the exception of the upper layers (0-5 cm) of SRS which showed a moist content of 2-6 %. LOI was found to be high in the upper layers of the sediment and decreased to below 10 % at a depth of 5-6 cm. For Sellafield (K2), LOI was 7 % at top layer and decreased to 3 % in the bottom layers. Tables in Appendix A.

2.3. Measurements

Radionuclides can be identified and quantified by radiometric and mass spectrometric methods, destructive and non-destructive, as well as by different analytical techniques for particle identification and particle characterization. Autoradiography and electron microscope provides non-destructive methods of particle identification and characterization. Radio-analytical techniques include non-destructive γ–spectrometry and destructive α-spectrometry. Mass spectrometric methods include inductively coupled plasma mass spectrometry (ICP-MS).

In the current work, measurements were performed to obtain information about ^{238}Pu, ^{239}Pu, ^{240}Pu, ^{241}Am and ^{137}Cs. ^{241}Am and ^{137}Cs was measured by gamma-spectrometry. ^{238}Pu activity was measured by alpha-spectrometry. Alpha-spectrometry also obtained information about $^{239+240}$Pu activity. ^{239}Pu and ^{240}Pu was measured by ICP-MS triple quadrupole, and obtained isotopic ratios of ^{240}Pu/^{239}Pu as well as ^{239}Pu and ^{240}Pu concentrations.

2.3.1. Identification, isolation and characterization of radioactive particles

Isolation, identification and characterization of radioactive particles requires the use of several analytical tools. The presence of radioactive particles can be determined by digital autoradiography, or by sample splitting with or without statistical tests. Characterization of particles can be performed by both non-destructive and destructive techniques. Examples of non-destructive techniques are analysis by ESEM-EDX or synchrotron (although this can be semi-destructive), and destructive techniques include SIMS, leaching experiments, mass spectrometry and alpha/beta spectrometry (Lind 2006).

Sample mixing and sample splitting

Radioactive disintegration can be described as a random process following the Poisson distribution. Mixing and counting of a sample with the presence of hot particles will after a number of mixings lead to the observed distribution not belonging to the same Poisson distribution. The procedure is extensively described in Bunzl (1998) and (Bunzl & Tschiersch 2001), and may lead to the assumption of the presence of inhomogeneous distribution.

H_0: all measurements belong to the same Poisson distribution

H_1: presence of inhomogeneous sample

$$z_i = 2(\sqrt{X_i + 1} - \sqrt{t_i \hat{\lambda}}) \qquad if \ \lambda_i^* < \hat{\lambda}$$

$$z_i = 2(\sqrt{X_i} - \sqrt{t_i \hat{\lambda}}) \qquad if \ \lambda_i^* > \hat{\lambda}$$

where X_i is number of counts observed, $\lambda_i^* = \frac{X_i}{t_i}$ and $\hat{\lambda} = \frac{\sum X_i}{\sum t_i}$. Counting time for each measurement is identical, so t_i is set to 1 and $\sum t_i$ = number of mixings m.

$$\widehat{\chi_i^2} = \sum_{i=1}^{m} z_i^2$$

If $\sum_{i=1}^{m} z_i^2$ for v = m-1 degrees of freedom is larger than tabulated value $\chi_{v, \alpha}$ from the χ^2-distribution at a given significance level α, H_o is rejected and the presence of inhomogeneous distribution must be assumed.

Repeated mixing and measuring was performed by Ge-detectors on Sellafield K2 25-30 (^{137}Cs and ^{241}Am) and SRS A9 7-8 (^{137}Cs). Sellafield K2 7-8 was contained in a low plastic box and weighed approximately 130 g. The sample was mixed and measured 10 times (measuring time 1245 seconds). The SRS A9 7-8 sample was contained in a 30 ml plastic vial and weighed approximately 16 g. The sample was mixed and measured 5 times (measuring time 430 s).

Another particle identification technique, sample splitting, is based on reducing a large sample size with high probability of catching a particle in the process. Comparing the sub-samples activities will provide information about significantly different activity concentrations present, which will indicate the presence of inhomogeneous distribution.

Sample splitting was performed for Sellafield K2 25-30 (^{241}Am and ^{137}Cs) and SRS A9 (^{137}Cs). Low levels of ^{241}Am in the SRS samples made it unsuitable to perform ^{241}Am measurements of the small sample sizes, due to time restrictions. The original K2 sample (23.1 g) was split in half and measured in Ge-detector. This was repeated three times with subsequent selection of the sub sample containing the highest activity. This selected sub sample was split in 10 equal

parts (sample size approximately 0.2 g) and measured for 4h in a NaI-detector. The procedure was identical for the SRS A9 7-8 sample (original sample size 16.5 g), but with 11 final sub samples (sample size approximately 0.2 g).

Digital P Imaging

Digital phosphor imaging (P imaging, also known as autoradiography) provides information about the presence and distribution of radioactivity within a sample. Exposure of the sample to a phosphorus plate enables transformation to an image, showing the original pattern of radioactivity. The imaging plate contains photostimulable crystals ($BaFBR:Eu^{2+}$), which traps and stores electrons excited by radioactive energy. The excited electrons are stored in the crystal lattice, until scanning of the plate with a laser beam releases the energy as luminescence (emission of light). Exposure times can be from 24 hours to several months, depending on the activity present in the sample. Detection limits of 2 mBq have been reported for ^{238}Pu particles (Zeissler et al. 1998). Application of autoradiography has shown to be useful in the identification of inhomogeneous distributions of radioactivity, and in the work of localizing radioactive particles.

Autoradiography was performed on samples from SRS (A9) and Sellafield (K2 and Ravenglass), with the purpose of detecting inhomogeneous distributions, as well as to isolate identified particles. A Molecular Dynamics Storage phosphorous screen, and a Typhoon 8600 Variable Mode Imager with Typhoon WM ware software was used. When hotspots were identified, further isolation was undertaken, to minimize the sample size before further investigations in ESEM.

ESEM-EDX – Environmental Scanning Electron Microscope and Energy Dispersive X-ray analysis system

A scanning electron microscope (ESEM-EDX) is useful to perform solid-state characterization of radioactive particles. Interactions between an electron beam and the specimen enables the creation of magnified two-dimensional images ranging from nm scale to μm scale, in addition to information regarding specimen composition. Secondary electrons (SE) and backscattered electrons (BSE) are used for obtaining images, as they provide information about structure and variation in composition, respectively. Characteristic X-rays emitted identifiy the specimen composition.

The signals that arise originate from SE, BSE, and characteristic X-rays. The SE-signal registers signals from the electrons ejected from the specimen surface atoms, and provides information about topography. The BSE-signal consists of high-energy electrons from the electron beam, which are reflected or elastically scattered by interaction with the specimen atoms. The registered signals are amplified and are presented as live images of the specimen, a back-scattered electron image (BEI) and a secondary electron image (SEI). Heavier atoms will backscatter electrons more easily than lighter ones, and appear more brightly colored in the BEI image. Suitable magnifications in images of specimen range from 10 – 10 000X, depending on the beam spot size.

Characteristic X-rays enables elemental identification and mapping of the sample (EDX), up to one µm in diameter and depth (Newbury et al. 2003). The electron ray excites electrons in atom orbitals in the samples, when they de-excite characteristic X-rays are emitted. A solid state X-ray detector converts the individual X-ray energies into electrical pulses corresponding to the characteristic X-ray of the present element (Goodge). The spectrum produced is presented as a plot of counts vs. energy (keV).

Localization and characterization of identified presence of particles was performed using a Zeiss EVO – 50 EP Scanning Electron Microscope (ESEM-EDX). The filament type is a tungsten (W) emitter, and the EDX system is an INCA Energy 350. The samples investigated were not coated.

2.3.2. Radio-analytical and mass spectrometry techniques

Gamma spectrometry

Gamma emitting radionuclides can easily be quantified by gamma-detector measurements, based on scintillation or semi-conductor principles. NaI-detectors consist of a cylindrical NaI-crystal and germanium detectors consists of a semiconductor material interacting with gamma radiation. Comparing the two, NaI-detectors provide better counting efficiency, while Ge-detectors provide better energy-resolution. Three processes influences the absorption of gamma rays in a NaI-crystal or a semiconductor material: photoelectric effect, Compton scattering and pair production. All three interaction processes cause attenuation of the photon beam as it passes through matter, so the sample material may act as an absorber of the signal. Also, gamma-measurements of low-level samples makes it important to minimize background radiation using

proper shielding, and to maximize counting efficiency. Maximizing counting efficiency in Ge-detectors requires application of optimal geometry in minimal distance from the detector.

Measurements were performed by a NaI-detector (Perkin Elmer Wallac Wizard 3" 1480 Automatic Gamma Counter) and two Ge-detectors (Ortec HPGe coaxial detector and Canberra GL 2020R LEGe detector, with Ortec GammaVision.software).

Extensive sample material from SRS made it necessary to limit the sample population, making the NaI-detector a preferable choice. Regression of ^{239,240}Pu and ^{241}Am on ^{137}Cs have yielded correlation coefficients of 0.98 (n=20), indicating that plutonium concentrations could be predicted from the more easily measured ^{137}Cs (Whicker et al. 1990). 271 samples (22 sediment cores) of varying weight, contained within 30 ml plastic vials, were analyzed for ^{137}Cs with a counting time of 5 min/sample. The criteria for subsequent selection of a sediment core were based on the presence of high activity as well as variation in depth profile, and sediment core A9 was selected for further analysis.

Ge- measurements of sediment cores K2 and A9 were also performed. Samples were counted for ^{137}Cs and ^{241}Am until counting uncertainty was below 5 %, where applicable. Introduction of correction factors based on standard solutions with ^{137}Cs and ^{241}Am, in addition to geometry corrections to adjust for self-absorption became necessary, as the quality assurance of the measurements did not provide satisfactory results. The results for Cs were still somewhat low after corrections, but they most probably provide uncertainties no higher than 20 %. Raw data and correction factors are listed in Appendix B and C.

Alpha-spectrometry
Alpha-spectrometry is a useful method to identify and quantify alpha-emitting radionuclides, as alpha particles exist in quantified energy levels, enabling identification of emitting nuclides present in the sample. Alpha-spectrometry has a low efficiency, making it necessary to measure low-level samples for a long period, up to weeks and even months. A limitation of alpha spectrometry arises due to interference from nuclides with overlapping α-energies, as is the case for ^{239}Pu and ^{240}Pu and

Measurements of ^{238}Pu and $^{239+240}$Pu were performed by a Canberra Alpha Spectrometer 7401. Sample selection was based on the goal to obtain ^{238}Pu/$^{239+240}$Pu ratios from the U.S, U.K. and Russia to illustrate different sources and operation modes. This was in addition to covering the whole range of $^{239+240}$Pu activity concentrations for comparison with ICP-MS measurements.

Based on these criteria seven samples were selected (A9 6-7 and 17-18; K2 2-4 and 25-30; Mayak 2626 and 3516; and IAEA 384). ^{238}Pu was not corrected for decay (ref. chapter 2.1.). Raw data is listed in Appendix D.

ICP-MS

Mass spectrometry enables separation of elements and isotopes by mass/charge ratio. This enables measurements of trace concentrations as in the case of environmental samples. Interferences in mass spectrometry arises from the presence of species with the same mass/charge ratio. Different techniques are applied to solve these problems. ICP-MS has the capacity to measure multiple elements in low concentrations. Rapid switching of voltage on the mass filter enables isotopic measurements. A number of different ICP-MS instruments exist, such as quadrupole, sector field, double focusing sector field, time of flight, and multi-collectors (Wendel 2014).

The ICP-MS triple quadrupole is a new ICP-MS instrument that shows promising possibilities. For instance, methods for isotope measurements of ^{129}I and determination of ^{134}Cs/^{137}Cs and ^{135}Cs/^{137}Cs have recently been obtained (Ohno et al. 2013; Ohno & Muramatsu 2014), which has been difficult when using conventional ICP-MS instruments. The analyte is introduced to the instrument as an aerosol or gas, and is transported by an argon carrier gas to a hot plasma (6000-8000K). Sample atoms are ionized and accelerated through the first quadrupole (Q1), where all masses except the analyte and on-mass interferences are discriminated (*Fig. 7*). This happens with the application of an electrical field through Q1 adjusted for the analyte mass, so Q1 acts as a mass filter. Then, a reaction/collision cell introduces a reactive gas such as CO_2, O_2, NH_3, or a mix, which reacts with ions by collisions to create molecules. Taking advantage of the atom reaction rates may enable the creation of molecules with either interference or analyte, enabling deflection of the interference by an electrical field in Q2. If the interference reacts and analyte does not, an on-mass detection is preferred. If the interference does not react and the analyte does, a mass shift detection is preferred. At low concentrations, atomic and polyatomic interferences are the limiting factor.

When measuring low-level environmental samples of plutonium, ^{238}U$^+$ interferes with ^{238}Pu, UH$^+$ interferes with ^{239}Pu, and UH$_2$$^+$ interferes with ^{240}Pu. UH$^+$ and UH$_2$$^+$ reacts with CO_2 to form UO$^+$ and UO$_2$$^+$. Lower reaction rates with Pu$^+$ allows sub ppt determination of ^{239}Pu, ^{240}Pu, and ^{242}Pu (less for ^{238}Pu) in the presence of seven orders of magnitude excess U matrix (Tanner et al. 2004).
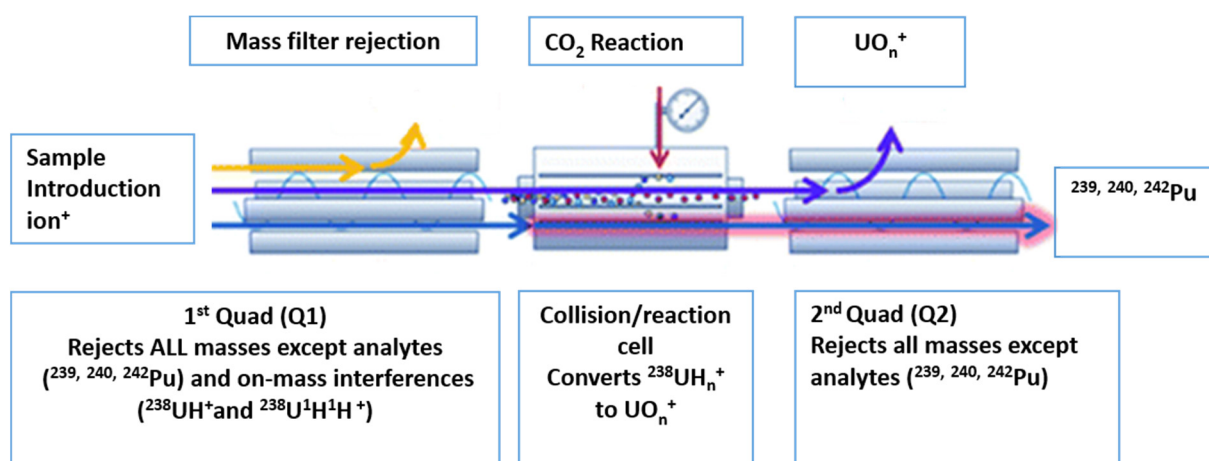
Figure 8. Operating principles of plutonium measurements by ICP-MS triple quadrupole (Balcaen et al. 2013).

In this work, $^{240}Pu/^{239}Pu$ isotopic ratios were obtained by mass spectrometry measurements using an Agilent 8800 ICP-MS triple quadrupole, as a part of a method development. Pu also reacts to PuO, and the method hardware was tuned for the highest possible signal with a 10 ppt ^{242}Pu solution to maximize the UO_n formation and minimize the PuO formation. 0.32 mL/min of CO_2 gave a good signal to noise for Pu vs. UH for 1µg/L U. The mass balance was set to 93 % (of 260 amu) for best sensitivity of Pu masses. Normally, a quadrupole is most sensitive at mid mass of quad (130 amu for 8800). By setting the mass balance to 93% (242/260), the quad is most sensitive for mass 242. ICP-MS settings for the method are listed in Appendix E and F. Raw data from measurements are listed in Appendix G and H.

2.4.   Statistical approach and quality assurance

The reliability and precision of the results are important to consider. They were assured by considering blanks and background spectras to provide detection limits, the tracer was checked for potential contribution of analyte, and introduction of certified and in-house reference material for quality control. Intercomparison of methods was introduced when different methods for measurements of the same analyte was used to check correlation of methods.

2.4.1. Error analysis and statistical approach

Uncertainties will always arise when performing measurements. Error analysis provides information and evaluation of such uncertainties. Consideration of uncertainties enables a better foundation to draw the correct conclusions, and identifies the possible needs to reduce the uncertainties. All experimental uncertainty is due to either random or systematic error. Experimental uncertainties that can be revealed by repeating the measurements are called random errors, and these are linked to precision while systematic errors, linked to accuracy, are caused by miscalibration of instruments.

In this work, all measurement uncertainties was taken into consideration, as well as uncertainties associated with weights, tracer and background.

Measurement uncertainties were based on counting uncertainties for α-spectrometry and γ-spectrometry ($\sqrt{counts}$). ICP-MS measurements provided standard deviations based on three replicates of the same sample solution. Weight calibration was performed. Variations in weights was quantified by measuring different certified weights 10 times and determining the standard deviation of the population. The uncertainties ranged from 10^{-5} - 10^{-4} for weights ranging from 1 – 30 g, and was assumed negligible for this work.

When combining uncertainties, propagated uncertainties were calculated. When adding and subtracting uncertainties, the sums and differences rule was applied. When multiplying or dividing uncertainties, the product and quotient rule was applied. Both formulas are listed below.

$$\sigma_{A \pm B} = \sqrt{\sigma_A^2 + \sigma_B^2}$$

$$\sigma_{AB \ or \ \frac{A}{B}} = \sqrt{(\frac{\sigma_A}{A})^2 + (\frac{\sigma_B}{B})^2}$$

Sample mean and population/corrected sample standard deviation were introduced in some cases, as well as weighted mean and weighted standard deviation. Calculation of sample mean and standard deviation is shown below, as well as population standard deviation:

$$\bar{x} = \frac{\sum_{i=1}^{N} x_i}{N}$$

$$s_{\bar{x}} = \sqrt{\frac{1}{N}\sum_{i=1}^{N}(x_i - \bar{x})^2}$$

$$s_{\bar{x}\,pop} = \sqrt{\frac{1}{N-1}\sum_{i=1}^{N}(x_i - \bar{x})^2}$$

Calculation of the weighted mean and weighted standard deviation is shown below:

$$\bar{x}_w = \frac{\sum wx}{\sum w}$$

$$s_w = \sqrt{\frac{\sum_{i=1}^{N} w_i(x_i - \bar{x}_w)^2}{\frac{N'-1}{N'}\sum_{i=1}^{N} w_i}}$$

where w_i is chosen weighing factor and N' is the number of non-zero weights.

To show existence of significant results, the standard deviation was set at 2σ to provide a 95% confidence interval where relevant. Experimental uncertainties were set to be in same order of magnitude as the result. All calculations of uncertainties were performed manually or by Excel.

Some uncertainties existed as to sampling times and sediment release times. For that reason, no results were decay corrected and reference date were set to 01.01.2015 for all measurements. A control was performed to check the impact of this choice. Correcting the value of the $^{137}Cs/^{239+240}Pu$ ratio to sampling date (2004) of sample K2 2-4 provided a ratio of 0.8 instead of 0.7, and did not affect the result to much.

2.4.2. Tracer

Investigation of the contribution of analyte from the ^{242}Pu tracer was performed to see if it was necessary to make adjustments of ^{239}Pu and ^{240}Pu results. This was done by plotting cps values of analytical blanks for $^{239,\,240}Pu$ against ^{242}Pu. If ^{242}Pu did contribute, one would expect some correlation to occur. It did not seem like the tracer made any significant contributions. Tables are presented in Appendix I.

2.4.3. Detection limits

The Limit of Detection (LOD) was calculated as described in Mocak et al. (1997). The LOD is defined as the lowest concentration level that can be determined to be statistically significant different from a blank. $LoD = \mu_b + 3\sigma_b$, where μ_b and σ_b is blank population mean and standard deviation, respectively.

The LOD for gamma was obtained from gamma software, and were between 20 mBq and 50 mBq for [241]Am and between 30 mBq and 60 mBq for [137]Cs. LOD for alpha was based on background spectra, and were between 11-16 mBq for [238]Pu, between 7-10 mBq for [239+240]Pu and between 5-12 mBq for [242]Pu . For ICP-MS, the mean population of blanks provided LOD, and were 115.5 fg (0.26 Bq/kg) for [239]Pu and 21.8 fg (0.18 Bq/kg) for [240]Pu.

The detection limits for ICP-MS measurements were calculated by finding the population mean and the population standard deviation of the blanks, respectively. Six analytical blanks were included, but for [240]Pu, one result was not available (N/A). Of the six analytical blanks included in the sample population, there was a strong suspicion of the presence of an outlier. Figures are presented in Appendix J. The application of Grubb's test to test for outliers in the blank population was based on the suspicion of one present outlier(Grubbs 1969). Grubb's test statistics are defined for the following hypotheses:

H_0: There are no outliers in the data set

H_1: There is one outlier in the data set

$$G = \frac{Y_{max} - \bar{Y}}{sd}$$

Where $\bar{Y}$ and sd is the blank sample mean and standard deviation, respectively. Application of Grubb's test rejected H_0, and accepted H_1 that one outlier was present by significance level $\alpha = 0.01$, and the blank was excluded. Test results are presented in Appendix J.

There exist several alternatives as to how to treat values below the LOD, since simple exclusion of data and treatment of the LOD may impact means and standard deviations by over- or underestimating (Wood et al. 2011). Substitution of LOD/2 is some places recommended as the new norm, however, it makes little difference as long as censoring intensity is small (less than 30%) (Zeghnoun et al. 2007). For ICP-MS measurements, only one sample was censored, which led to a censoring intensity of about 3 %. Furthermore, the sample had a small sample size (~ 0.3 g). Hence, SRS A9 3-4 was excluded from the ICP-MS results.

2.4.4. Reference material

Suitable reference material was included in the sample population for quality assurance of methods and results. Selected reference material in the sample population was IAEA300 Baltic Sea sediment, IAEA384 Fangataufa sediment, NIST4353 Rocky Flats soil, in-house standards Mayak 2626 sediment and Mayak 3516 soil, IAEA135, and IAEA373. Certified reference material values were compared to results from ICP-MS, gamma-spectrometry and alpha-spectrometry.

For the ICP-MS measurements, selected reference material was IAEA384, IAEA300, NIST 4353, and in house standards Mayak 2626 and 3516 (*table 4).* All measurements of isotopic ratios were within the limits of corresponding uncertainties and 95% CI. The reference dates were not adjusted, as it was not necessary due to the long half-lives of ^{239}Pu and ^{240}Pu. In general the isotopic ratios obtained from this work lies higher than certified values and values from other work used here. Certified reference material for isotopic ratios should have been used for correction, but was not available. IAEA384 has a ^{239,240}Pu activity concentration corresponding with certified values, but the ^{239}Pu activity concentration lies outside the limits of uncertainties listed by Godoy et al. (2009). For IAEA 300 the ^{239}Pu and ^{240}Pu activity concentration of current work lies without the limits of uncertainty compared to values listed by Nassef et al. (2008). It should be noted that sample size of IAEA 300 was only ~ 0.7 g.

Table 4. Certified reference material and comparison with ICP-MS results (95% CI included for some certified values of activity concentrations).

Reference material	^{239}Pu Bq/kg	^{240}Pu Bg/kg	$^{239+240}$Pu Bq/kg	^{240}Pu/^{239}Pu ratio	Reference	Reference date
IAEA 384 Fangatufa sediment	98 CI: 85-105	17.5 CI: 15.1-18.7	107 CI: 103-110	0.049±0.001	Referencesheet	01.08.1996
	94.67±0.63	17.35±0.12	112.02±0.74	0.050±0.001	(Godoy et al. 2009)	01.08.1996
	88.53±5.24	17.65±3.12	106.2±6.10	0.054±0.009	This work (n=2)	01.01.2015
IAEA 300 Baltic Sea Sediment			3.55 CI: 3.44-3.65		Reference sheet	01.01.1993
	0.184±0.004	3.38±0.08		0.19±0.02	(Nassef et al. 2008)	01.01.1993
	1.75±0.18	1.43±0.28	3.18±0.33	0.22±0.05	This work (n=1)	01.01.2015
NIST 4353 Rocky Flats soil			16.8 CI: 6-26.8	0.056 CI:0.053-0.06	Referencesheet	01.04.1998
	9.45±0.44	2.05±0.22	11.5±0.5	0.059±0.006	This work (n=1)	01.01.2015
In-house Standard 2626 Mayak sediment				0.115±0.007	(Wendel 2014)	01.01.2014
				0.127±0.004	(Wendel 2014)	01.01.2014
	10.4±0.8	4.78±0.49	15.18±0.94	0.124±0.016	This work (n=1)	01.01.2015
In-house Standard 3516 Mayak soil				0.0194±0.001	(Wendel 2014)	01.01.2014
				0.019±0.003	(Wendel 2014)	01.01.2014
	23.52±0.91	1.92±0.34	25.45±0.97	0.022±0.004	This work (n=1)	01.01.2015

Quality assurance for Ge-detector results was performed by comparing results from measured reference material IAEA135 (with different geometries and calibration factors for both detectors), and IAEA373 with certified values (*table 5*). Reference values were corrected for decay where needed (^{137}Cs). The values for detector 1 fits the reference material best, although they do not completely correspond to reference values within the limits of uncertainty. ^{241}Am reference values are not correct, as one would expect ingrowth from ^{241}Pu. Certified values for ^{241}Pu were not found. Calibration was performed to assure the quality of the results but did not provide results within the limits of uncertainty for both detectors and all calibrations. Even so, it is assumed that uncertainties of ^{137}Cs and ^{241}Am results do not exceed 20%.

Table 5. Certified reference material and comparison with results from gamma measurements compared for quality assurance, reference date 01.01.2015.

Reference material	^{137}Cs (Bq/kg)	^{241}Am (Bq/kg)	Reference	Geometry
IAEA 135	653 (640 - 678)	318 (310-325)	Reference sheet	
	641±19	498±8	Current work (detector 1)	5ml
	744±22	555±8		10ml
	646±26	494±9		15ml
	577±20	484±45	Current work (detector 2)	5ml
	600±26	499±36		10ml
	618±25	490±20		15ml
IAEA 373	7281 (7151 - 7410)		Reference sheet	
	7738±218		Current work	

For alpha-spectrometry, IAEA384 was selected as reference material for quality assurance (*table 6).* The results were in consistency with certified values within the levels of uncertainty.

Table 6. Certified values of IAEA384 and comparison with alpha spectrometry results for quality assurance, reference date 01.01.15.

Reference material	^{238}Pu (Bq/kg)	$^{239+240}$Pu (Bq/kg)	^{238}Pu/$^{239+240}$Pu ratio	Reference
IAEA 384	36 (CI: 32.8 – 34.5)	107 (CI: 103-110)	0.313±0.08	Reference sheet
	27.9±8.6	93.1±27.7	0.312±0.03	This work (n=1)

2.4.5. Intercomparison of methods

A comparison of gamma measurements from the NaI-detector and Ge-detector was performed for ^{137}Cs with the SRS A9 samples, which showed good correlation (R^2=0.9765) even though a spread was observed for higher energies, probably caused by miscalibration (*Fig. 9)*. Measured activities were not 1:1, which was probably influenced by the NaI detector not having a factor for self-absorption.
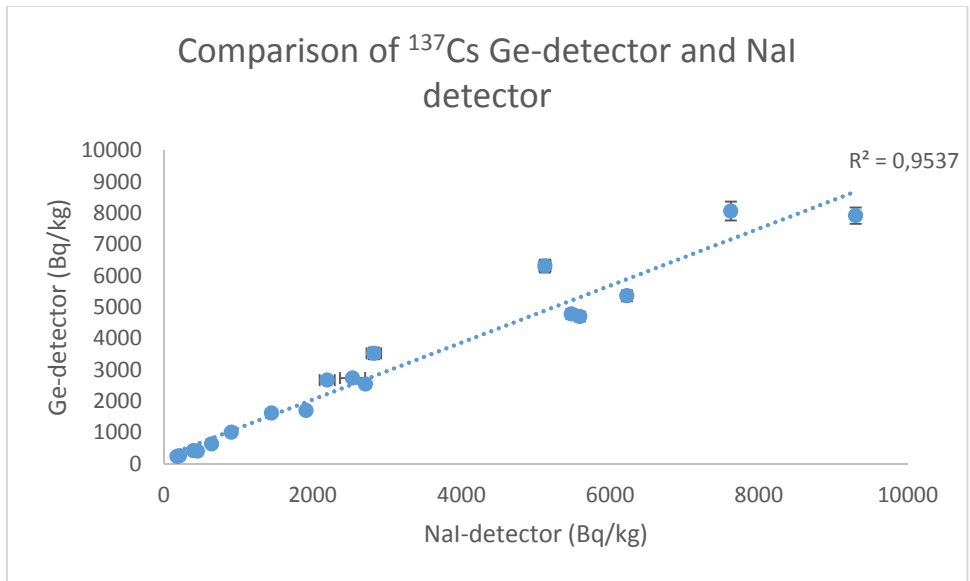
Figure 9. Comparison of methods for gamma measurements, Ge-detector vs. NaI-detector.

Comparison of $^{239+240}$Pu activity ratios obtained by ICP-MS and alpha-spectrometry respectively, showed a very strong correlation, with $R^2 = 0.9999$ (*Fig. 10)*. Removal of the two top points still yielded a very strong correlation with $R^2 = 0.9998$.
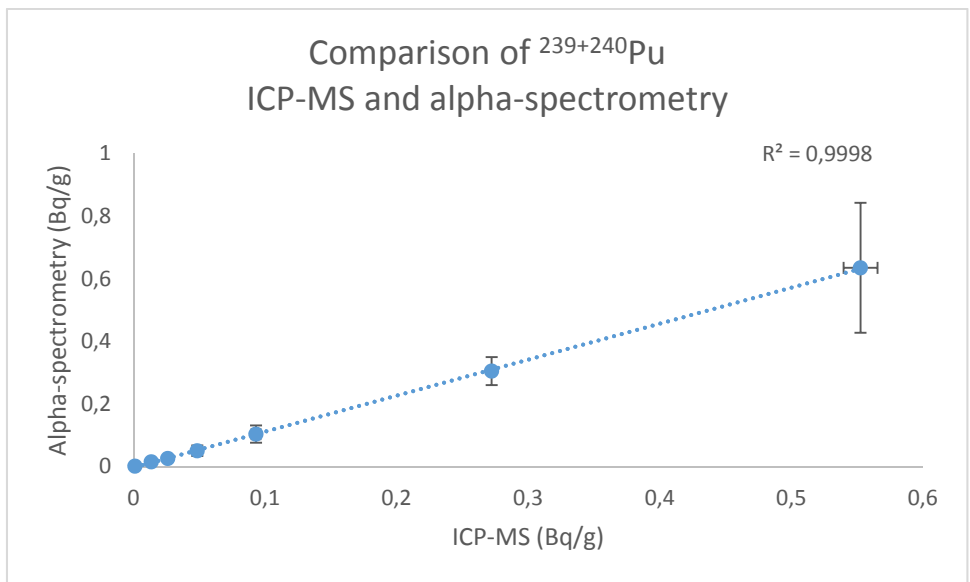

Figure 10. Comparison of $^{239+240}$Pu activity ratios obtained by ICP-MS triple quadrupole and alpha-spectrometry.

3. Results & Discussion

In the present work, activity concentrations of ^{238}Pu, $^{239,\,240}$Pu, ^{241}Am and ^{137}Cs have been determined using gamma and alpha spectrometry. The detection limits for gamma were between 20 mBq and 50 mBq for ^{241}Am and between 30 mBq and 60 mBq for ^{137}Cs. The detection limits for alpha were between 11-16 mBq for ^{238}Pu, between 7-10 mBq for $^{239+240}$Pu and between 5-12 mBq for ^{242}Pu. Different spectras were obtained for gamma and alpha measurements, some listed in Appendix J.

In addition, Pu isotopes (^{239}Pu and ^{240}Pu) were determined by ICP-MS. Prior to analysis, radioactive particles were identified using P imaging and ESEM. Information on particle characteristics were obtained using a combination of P imaging and ESEM-EDX. For P imaging, detection limits of 2 mBq has been reported for ^{238}Pu particles (Zeissler et al. 1998).

The measurements of ^{239}Pu and ^{240}Pu were performed as a part of a method development procedure for determination of ^{240}Pu/^{239}Pu isotopic ratios on the Agilent 8800 ICP-MS triple quadrupole. In the current procedure varying signal due to the use of acid washed glasses, several steps with evaporation, redissolution, and sample uptake in different solutions contributed to overall uncertainty. The method was optimized to reduce interference from UH^+ peak in the ^{239}Pu peak, and lower CO_2 injection could probably improve the Pu sensitivity.

The procedural detection limits were 115.5 fg (0.26 Bq/kg) and 21.8 fg (0.18 Bq/kg) for ^{239}Pu and ^{240}Pu, respectively. Corresponding instrumental detection limits were 9.0 fg and 1.6 fg. The procedural LOD led to exclusion of one measurement (SRS 3-4). Other work with ICP-MS has given detection limit of 10-15 fg for plutonium (Skipperud 2004), and 265 fg and 74.5 fg for ^{239}Pu and ^{240}Pu, respectively (Wendel 2014). Comparison of procedural detection limits obtained by others show that ICP-MS triple quadrupole is a promising method for the determination of plutonium, as the obtained detection limits lies lower than recently obtained with sector field ICP-MS, although higher than obtained with ICP-MS quadrupole by Skipperud (2004). The method can currently not compete with AMS, with detection limits of 4.2 fg and 1.3 fg for ^{239}Pu and ^{240}Pu, respectively(Wendel 2014).

3.1. Radioactive particles

3.1.1. Particle identification

Sample splitting

Sample splitting and subsequent gamma measurements were performed for SRS (A9 6-7) and Sellafield (K2 25-30). For Sellafield K2, there were indications that ^{137}Cs inhomogenities were present, as measurements of sub samples showed that the activity in two samples (sample 5 and 6) were significantly different from each other (*Fig. 11*). The result showed that the activity was not evenly distributed throughout the sample. No significant differences in the gamma activity were obtained for the other samples.
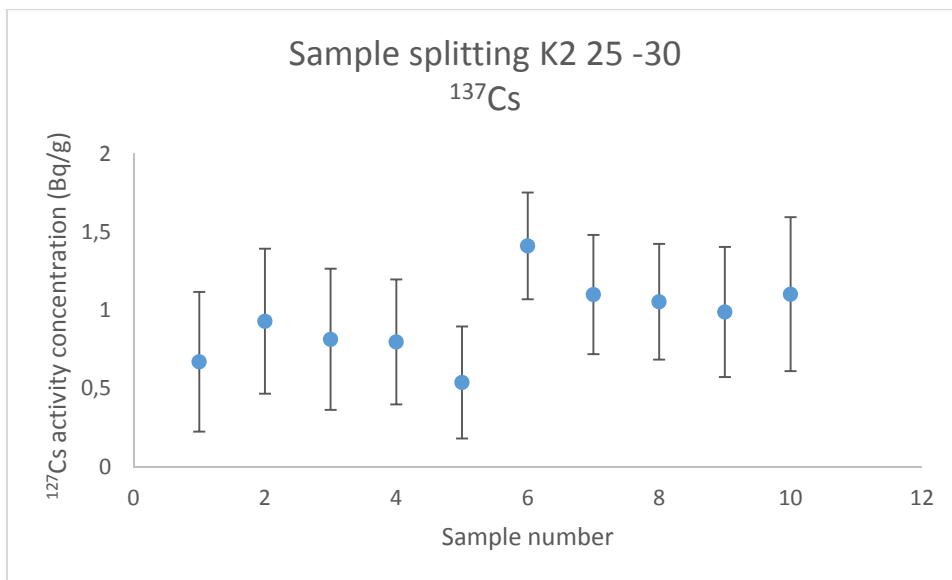

Figure 11. Sample splitting K2 25-30 (Uncertainties set to two sigma for significance level α=0.05)..

Repeated mixing and subsequent gamma measurements

Repeated mixing, subsequent gamma measurements by Ge-detector and application of chi-square test (χ^2 test) for the SRS A9 7-8 cm and Sellafield K2 25-30 cm indicated the presence of inhomogeneous activity distributions. The resulting test provided significant results for ^{137}Cs (SRS A9) and for ^{241}Am (Sellafield K2) (*table 7*). For SRS, the calculated value of $\hat{\chi}^2$ (11.61) was higher than the tabulated value (9.49) for a significance level of α = 0.05, so rejection of H$_0$ and acceptance of H$_1$ indicated that homogenously distribution is present is given by 95% certainty.

For Sellafield K2, the calculated value of $\hat{\chi}^2$ (72.84) was higher than the tabulated value (27.88) for a significance level of $\alpha = 0.001$, so rejection of H_0 and acceptance of H_1 that homogenously distribution is present is given by 99.9 % certainty.

The test did not provide significant results for Sellafield K2 25-30 cm for [137]Cs. The sample size was big, and the sample containment was low, so probably, too many particles were present causing an even distribution. Since significant results were produced by [241]Am, another explanation may be that the much smaller attenuation coefficient for 661,61 keV made it harder to separate the changes in particle location.

Table 7. $\hat{\chi}^2$- test for identification of presence of radioactive inhomogenities (df: degree of freedom).

Sample	Isotope	df	Significance level and tabulated values of $\hat{\chi}^2$			Calculated $\hat{\chi}^2$
			0.05	0.01	0.001	
SRS A9 7-8	[137]Cs	4	9.49	13.28	18.47	11.61
K2 25-30	[241]Am	9	16.92	21.67	27.88	72.84

Autoradiography

Results from autoradiography for SRS (A9) and Sellafield (K2 and Ravenglass) indicated the presence of radioactive particles. Autoradiography of SRS A9 sediments with a long exposure time (6 weeks) provided clear indications of the presence of radioactive particles (*Fig. 12*). Hotspots were also observed for shorter exposure times, approximately 5 days. The presence of heterogeneities were confirmed, however, it was not possible to isolate and confirm the presence of radioactive particles.

Figure 12. Digital autoradiography of Savannah River Site sediments Pond A 0-7 cm (6 weeks exposure).

Autoradiography of Sellafield (K2 and Ravenglass) sediment also provided clear indications of the presence of radioactive particles (*Fig. 13)*, and a shorter exposure time than the Savannah sample was required. The Sellafield hotspots provided the strongest signal, and required the shortest exposure time. Sellafield K2 sediment contained 1 hotspot/gram sample (all sediment layers combined), and Ravenglass had approximately 40 hotspots/gram.
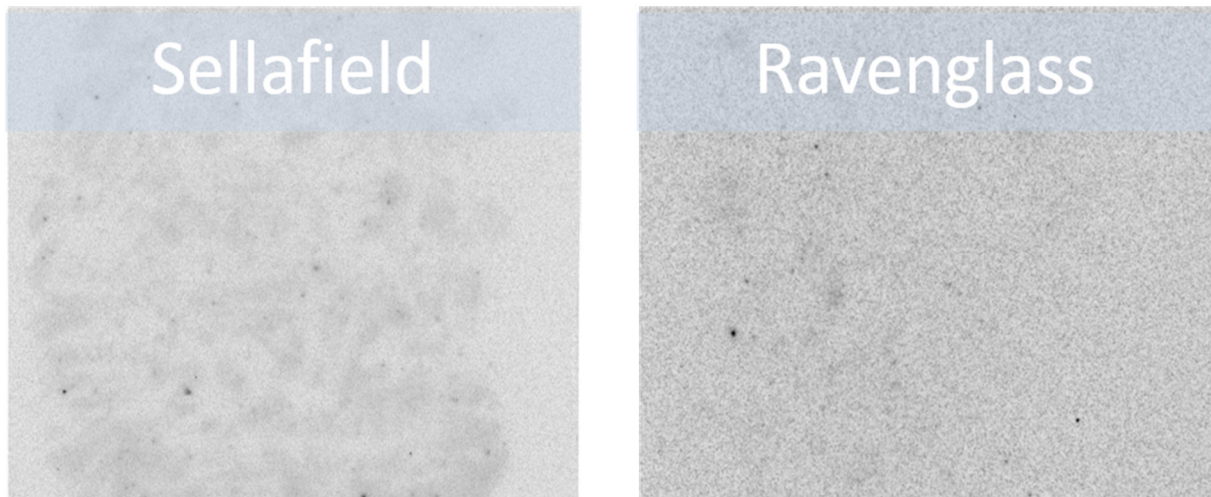

Figure 13. Left: Digital autoradiography of Sellafield K2 sediment 0-30 cm, 24h exposure; right: digital autoradiography of Ravenglass surface sediment, 72h exposure.

Earlier work by Lind (2006), has shown indications of the presence of radioactive particles in all sediment layers from Sellafield K2 (*Fig. 14)*.
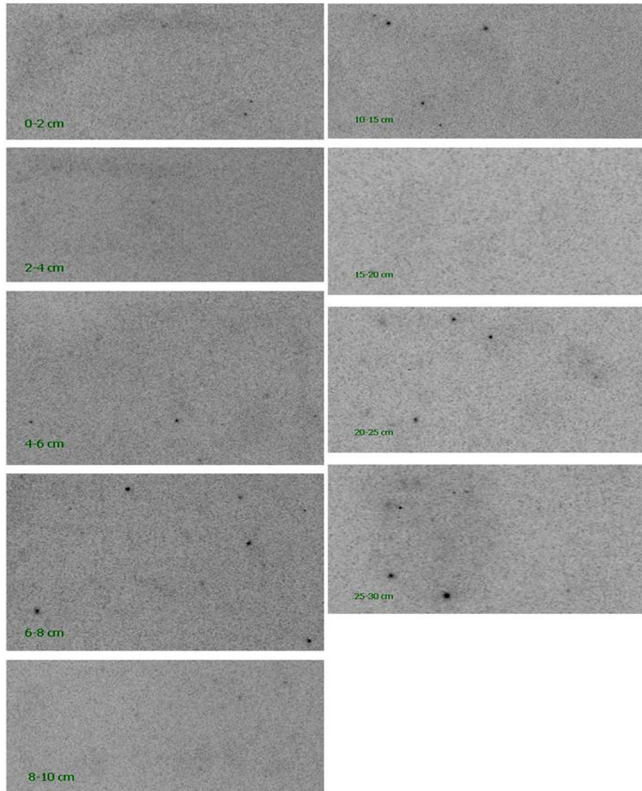

Figure 14. Digital autoradiography of sediment core K2 (0-30 cm) (Lind 2006)

Particle isolation was performed for SRS and Sellafield (K2 and Ravenglass) *(Fig. 15)*. The two hotspots from Ravenglass were later identified as uranium particles by investigations in ESEM-EDX.
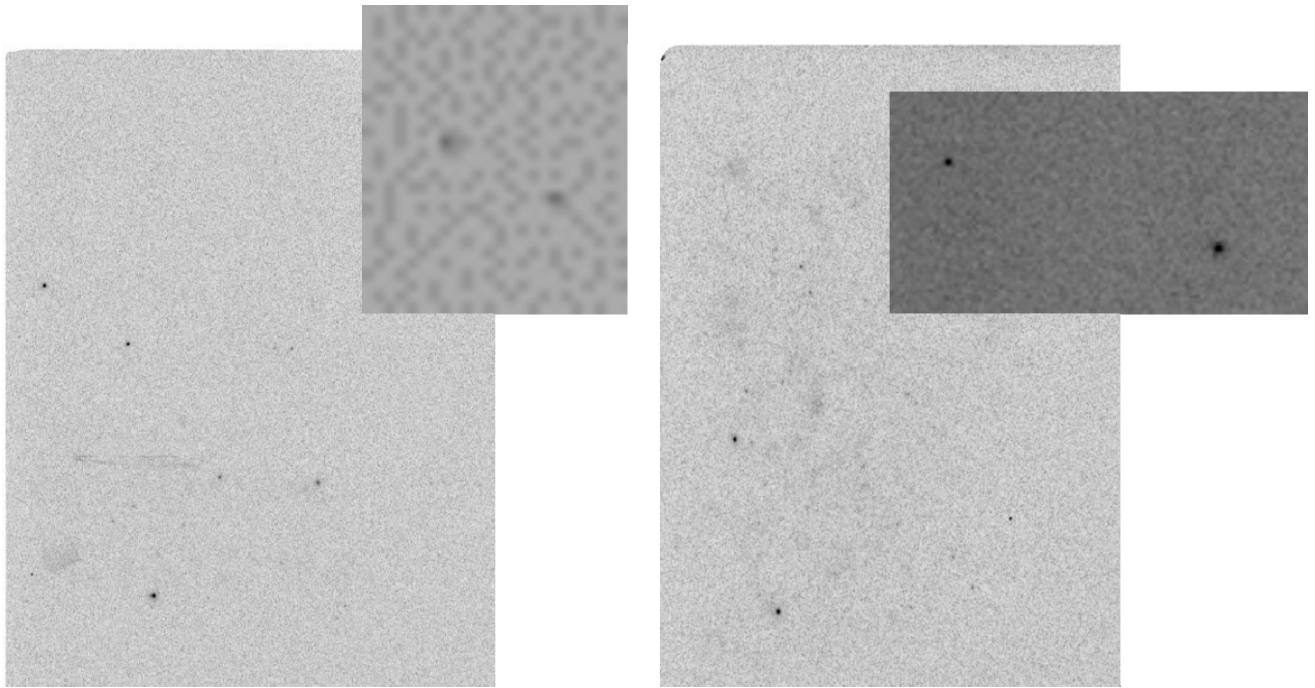

Figure 15. Particle isolations Sellafield K2 0-30 24h exposure (left); Particle isolations Ravenglass 24h exposure (right).

3.1.2. Particle characterization

Uranium particles from Sellafield – Ravenglass were identified by ESEM-EDX (*Fig. 16*). The left image shows the sample (SEI-mode) with an isolated particle, and the right image (BEI-mode) shows the light spots from electron beam backscattering caused by the presence of uranium atoms.
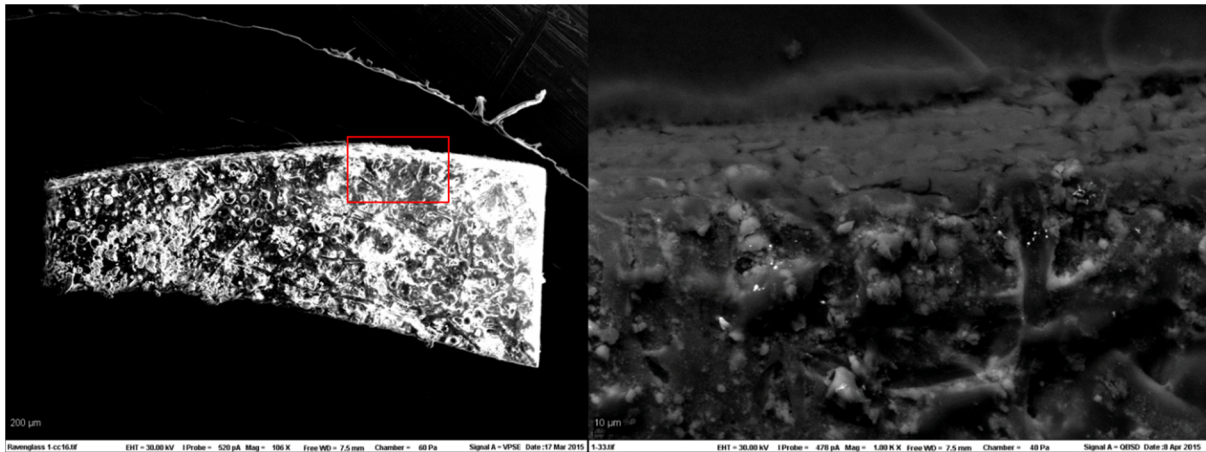
Figure 16. Sample image in SEI-mode (left image); Uranium clusters identified by BEI-mode image (right image).

BEI-images were produced of the two uranium clusters by magnifying 6500 and 9000 times, respectively, and XRMA- spectra confirmed the presence of uranium (*Fig.17*). Earlier work have confirmed the presence of U fuel particles in the Irish Sea ((Jernström 2006; Lind 2006)

Figure 17. Top image: Uranium clusters magnified in BEI mode; bottom image: XRMA-spectrum.

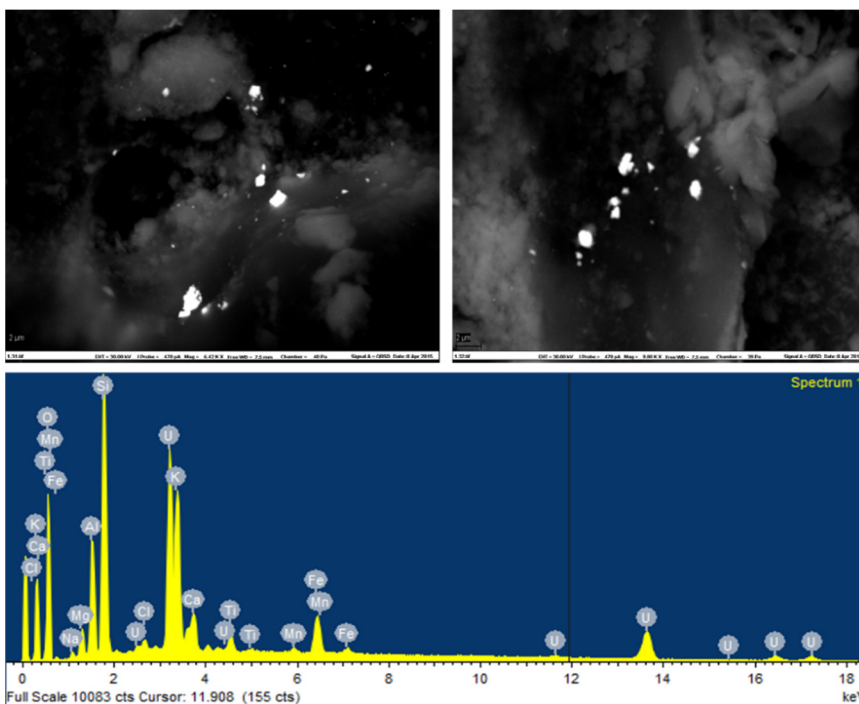Determination of the size distribution of identified uranium particles from Sellafield (Ravenglass) was performed (*Fig. 18*). The size distribution ranged from sub-µm to 2µm, with the sub-microns dominating in numbers. Colloids and particles are assumed to settle in sediment. However, transformations over a long time scale may contribute to remobilization and transport to the water phase (Vintró et al. 2000). In this work, particles and colloids/nanoparticles were observed as incorporated in the sediment, and did not imply any signs of remobilization. Sellafield derived particles has been identified transported to adjacent beaches and to intertidal sediments dependent on their size (Ltd. 2014). It is believed than fine coarsed particles will follow the current northward from Sellafield and deposit in the intertidal sediments, and these findings corresponds with those beliefs.
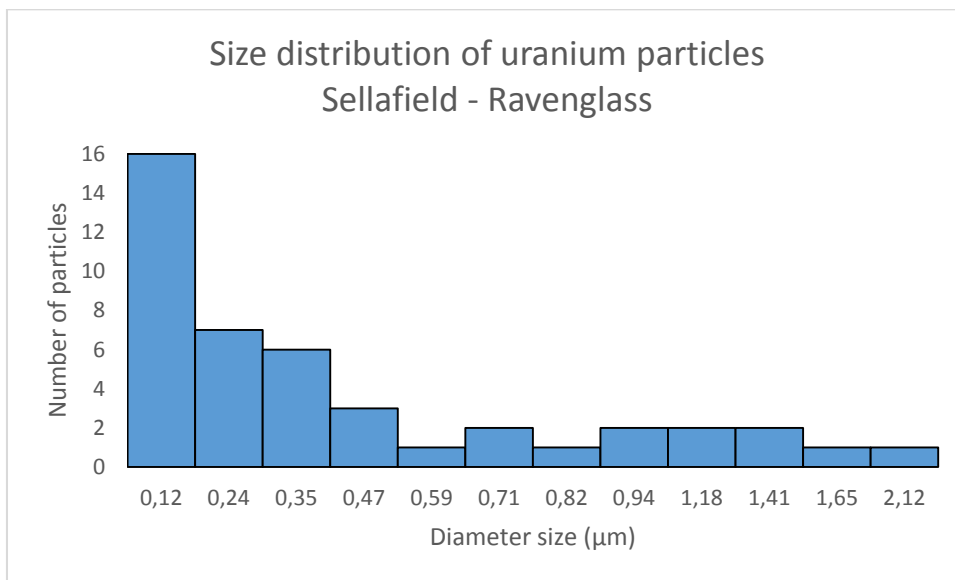

Figure 18. Size distribution of 44 uranium particles/colloids from Sellafield (Ravenglass) sediment identified with ESEM-EDX.

3.2. Sample screening Pond A

Measurements of ^{137}Cs by NaI-detector provided a rapid overview of variation in the depth profiles of the available sediment cores, and since strong correlation is expected between ^{137}Cs and plutonium, the Cs distribution should identify which of the cores should be most interesting for further analysis of Pu.

The sediment core A9 showed a different distribution than the others (*Fig. 19a),* with a peak at 7-8 cm depth suggesting a change in release history. Thus, A9 was selected for further sample-treatment and subsequent plutonium analysis together with Sellafield K2 and selected reference material. The overall ^{137}Cs peak activity occurring at ~ 2-4 cm corresponded well with findings in previous work ((Abraham et al. 2000; Whicker et al. 1990).

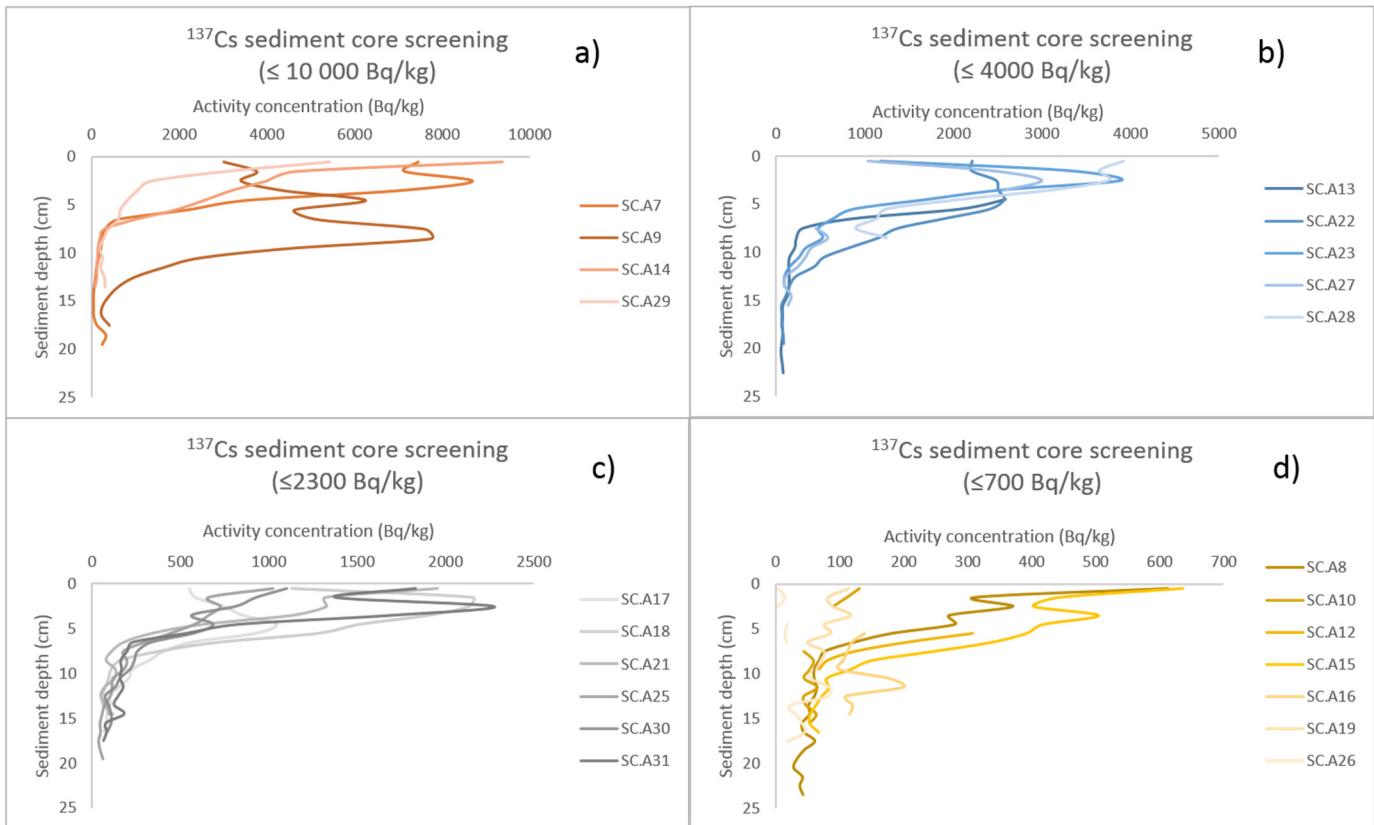*Figure 19. Screening of 22 sediment cores from SRS Pond A performed by NaI-detector. a) sediment cores with peak activity concentrations ranging from 4000 – 10 000 Bq/kg; b) sediment cores with peak activity concentrations ranging from 1000 – 4000 Bq/kg; c) sediment cores with peak activity concentrations ranging from 500 – 2300 Bq/kg; d) sediment cores with peak activity concentrations ranging from 0 - 700 Bq/kg.*

3.3. Activity concentrations

The depth distributions of ^{137}Cs, ^{241}Am, and $^{239+240}$Pu activity concentrations have been determined in the sediment cores from Savannah River Site and Sellafield (K2).

Savannah River Site

The upper sediment layers at SRS core A9 have a ^{137}Cs activity concentration of approximately 2000 Bq/kg. The depth distribution show a peak at 7-8 cm depth (*Fig. 20)*, and the peak value was within 9000–10 000 Bq/kg. The distribution corresponds with previous findings from Pond B, core B10 (Whicker et al. 1990), although the authors reported a three times higher peak activity concentration (approximately 30 000 Bq/kg). ^{241}Am concentrations were then showed to be approximately half of the $^{239+240}$Pu levels, indicating expected ^{241}Am levels in Pond A samples to be less than 50 Bq/kg. The ^{241}Am levels in provided samples from SRS were very low, close to or below the detection limit, in agreement with earlier work (Whicker et al. 1990).

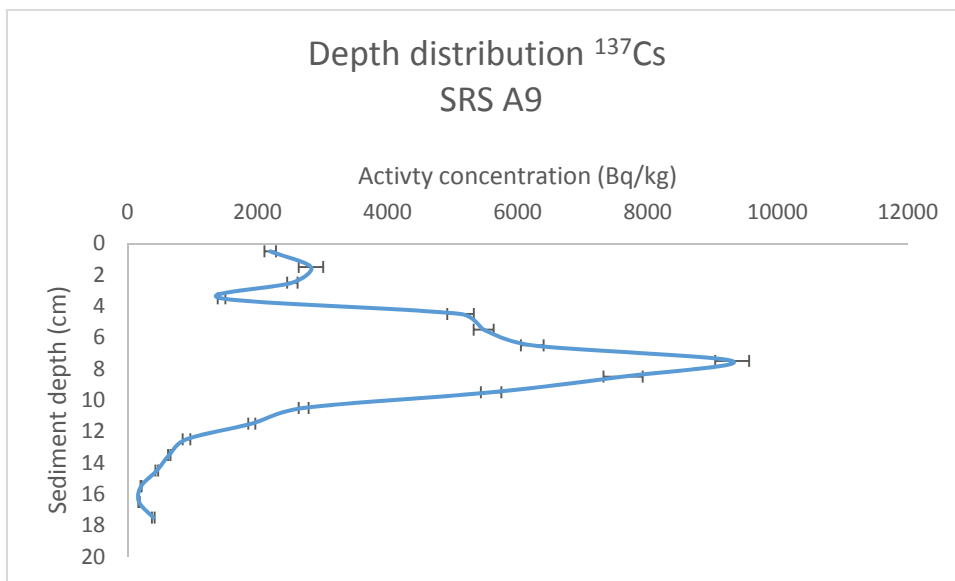*Figure 20. Depth distribution of ^{137}Cs SRS A9.*

The depth distribution of $^{239+240}$Pu in Pond A show peak activity at the depth 6-7 cm, of approximately 50 Bq/kg (*Fig. 21*). The distribution corresponds with earlier findings in Pond B, core B10 (Whicker et al. 1990), having a peak in the 8-9 cm sediment depth (45 Bq/kg), although the activity concentration found in Pond A, core A9, was somewhat higher.

53

The concentration did not decrease below the detection limit for the bottom sediment layers. However, most of the contamination seems retained in the upper parts of the sediment.

Comparison with other work done at Pond B, indicates that a larger portion of the ^{137}Cs was transferred to Pond B, while a larger portion of $^{239+240}$Pu was retained in Pond A. This corresponds with the assumption that Pu is settling in a higher rate than Cs, especially in the presence of organic material as is the case in Pond A. Loss on ignition showed a high content of organic material in the upper sediment layers at Pond A. TOC is known to reduce Pu to its more stable and particle reactive form (III or VI), and can be strongly associated with carbonate or organics (Neu et al. 2011).
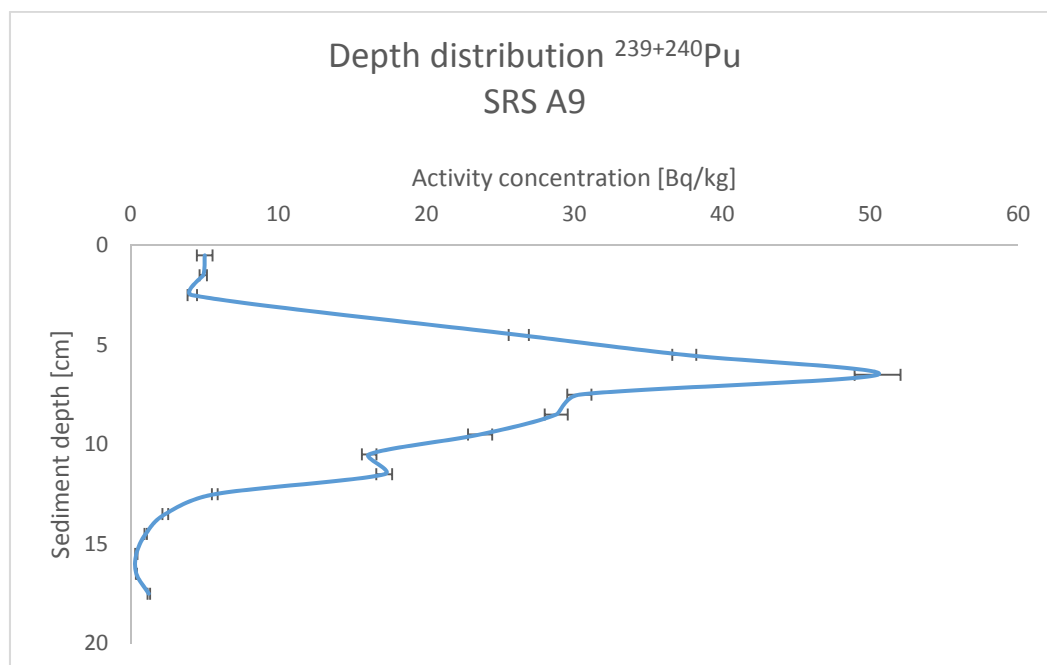
Figure 21. Depth distribution of $^{239+240}$Pu, SRS A9.

Sellafield

The depth distribution of ^{137}Cs and ^{241}Am in the Sellafield core (K2) showed low concentrations of ^{137}Cs (200-500 Bq/kg), and significantly higher ^{241}Am concentrations (1000-2000 Bq/kg) (*Fig. 22*). This could reflect differences in release, in deposition or differences in mobility within sediment. The calculated ^{137}Cs/^{241}Am ratio for total releases from Sellafield between 1952-98 is ~76 Vintró et al. (2000), while the present results are significantly lower (≤ 1).

This is as expected as it is shown that ^{137}Cs is relatively soluble in seawater and is advected northward (Vintró et al. 2000). Both radionuclides peak in the deeper layers. The distribution corresponds with findings in the EU founded Remotrans project (2004), although the compared results were based of intertidal sediments, and showed a higher concentration in the bottom sediment layers (peak value of 6000-7000 Bq/kg for ^{137}Cs and ^{241}Am, respectively). Horizontal movement and vertical mixing of sub-tidal sediment has been shown (Kershaw et al. 1999) and may also explain the decrease in concentration in the eastern Irish Sea sub-tidal sediments compared to intertidal sediments.
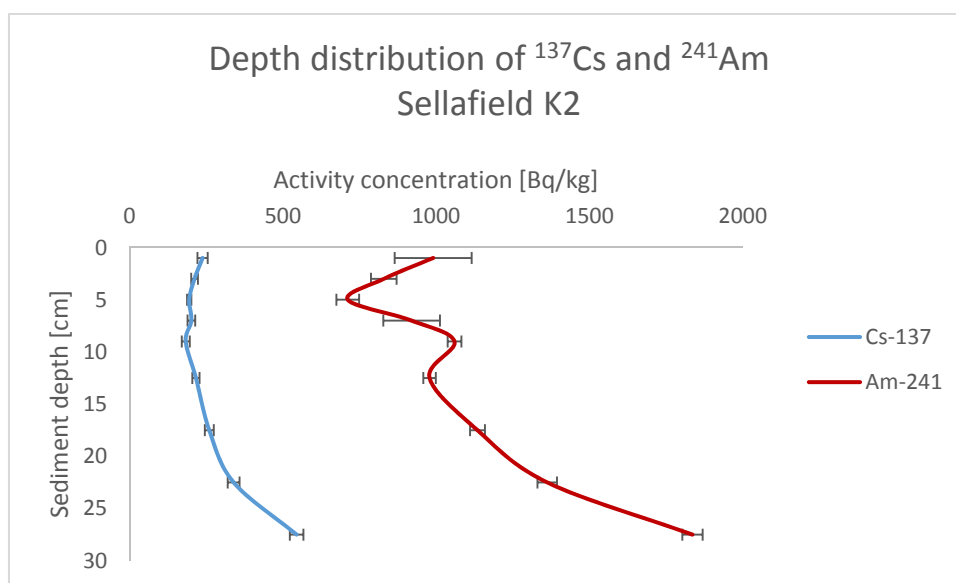
Figure 22. Depth distribution of ^{137}Cs and ^{241}Am Sellafield K2.

The depth distribution of $^{239+240}$Pu in the Sellafield K2 core showed a $^{239+240}$Pu concentration that did not vary a lot by depth, but ranges within 300-400 Bq/kg (*Fig. 23*). This corresponds with findings from Remotrans (2004) in the upper 15 cm layers. The compared data originates from an intertidal sediment core and showed a higher concentration in the lower layers (1000-6000 Bq/kg) than in the current work, where it in the deepest increment (25-30 cm) was observed a rapid increase in concentration to 600-700 Bq/kg. As mentioned earlier, this may be explained by vertical movement of sub-tidal sediment or due to the fact that the previous releases of Pu was rather high.

Figure 23. Depth distribution of $^{239+240}$Pu, Sellafield K2.

Sedimentation rates in Sellafield sediments are in earlier work found to be low ($\sim$ 1mm/y) (Kershaw et al. 1999). The EARP (Enhanced Actinide Remover Plant) was put into operation in 1994, and reduced the release of actinides more efficiently (Vintró et al. 2000; Wendel 2007). Twenty years of sediment growth would only lead to an increase in sediment by 20 mm, and does not explain the increase in actinide concentrations at the 20 cm depth.

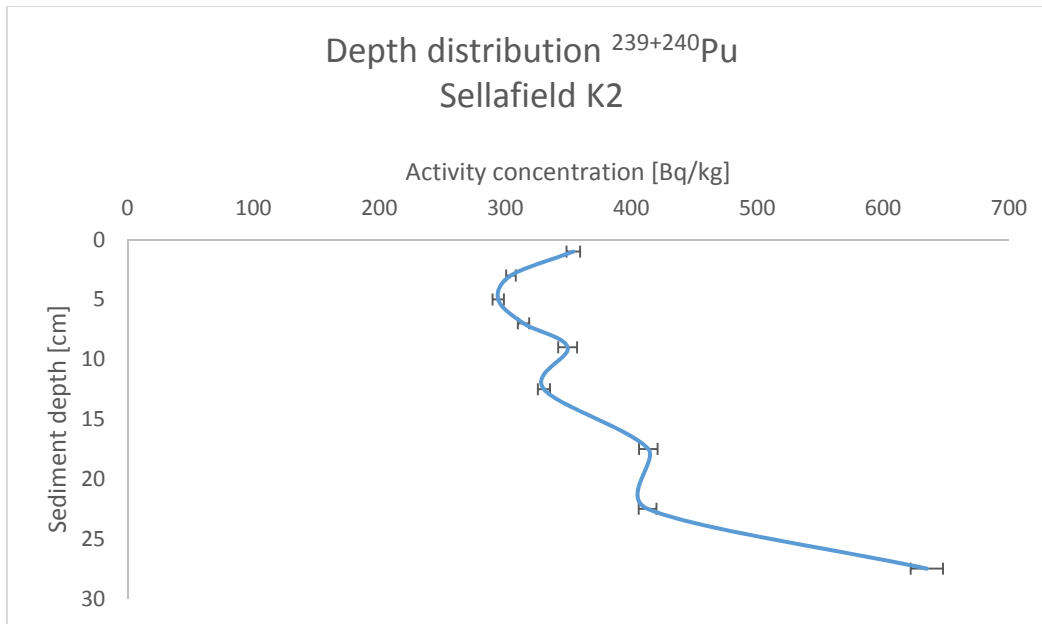Concentration profiles from this work is comparable with other findings when it comes to depth distributions. The intertidal sediment core from the DIAPLU collaboration show peaks in depths comparable with current findings for both ^{137}Cs, ^{241}Am and $^{239+240}$Pu.

For SRS, the work of Whicker et al. (1990) at Pond B has shown to be comparable to the results from current work in Pond A.

The low ^{137}Cs levels in the Sellafield K2 core compared with SRS is somewhat surprising. Rough estimates of the discharges of ^{137}Cs to Pond A are approximately 150 TBq, while the Sellafield discharges are estimated to be 41 TBq (Vintró et al. 2000). The difference in discharge history do not reflect the difference in depth distribution shown in this work, as it is 4-20 times higher at SRS compared to Sellafield (K2). This can possibly be explained by the high solubility of ^{137}Cs in sea water at Sellafield (Vintró et al. 2000), as well as extensive down core mixing, as the historical discharges should not be reflected at shallow sediment depths. The much higher levels of ^{137}Cs in the SRS core may also be explained by favoring retention in fresh water sediments or in soils situated in shallow waters, as reported in Carlton et al. (1994), as the Pond A has been an undisturbed lake without river in- or output.

3.4.   Source identification

Information on activity ratios and isotopic ratios is helpful when estimating the inventory of radionuclide contamination, and can be utilized to identify sources and reveal information about historical discharges. Different sources can be identified by their characteristic Pu isotopic ratio, which vary with factors such as nuclear burn-up, reactor type and reprocessing history. Weapons grade Pu is characterized by a low ^{240}Pu/^{239}Pu ratio compared to the global fallout ratio, while Pu originating from nuclear energy production is characterized by a higher isotopic ratio compared to the global fallout ratio. Information on isotopic ratios can also identifiy the influence of different sources contributing to the overall radioactive contamination. Combining ^{240}Pu/^{239}Pu isotopic ratio and ^{238}Pu/$^{239+240}$Pu activity ratio can be utilized for source term identification that otherwise can be hard to distinguish. Calculations of Pu isotope ratios are listed in Appendix K.

Activity ratios

The depth distribution of ^{137}Cs/$^{239+240}$Pu activity ratio for SRS A9 showed large variations, with range 100 - 600 (*Fig. 24*). For comparison, the global fallout ratio of ^{137}Cs/$^{239+240}$Pu (obtained from Japan, since Europe and Norway are affected by the Chernobyl accident) is ranging between 28 and 37 (Sakaguchi et al. 2009). Events in 1957 and in 1964 caused abnormal releases to seepage basins, which could possibly explain the two peaks, but according to literature Pond A did not receive discharges in 1957. It is, however, reasonable to believe that the peak in the upper sediment layer is influenced by the event in 1964, right before R-reactor closed down and the discharges ended.
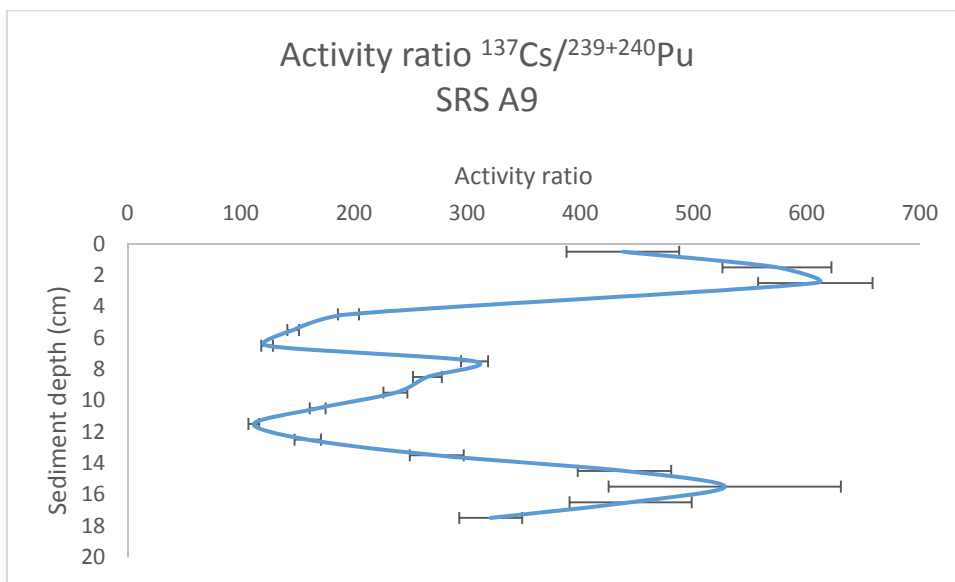

Figure 24. ^{137}Cs/$^{239+240}$Pu activity ratio SRS A9 (ref.date 01.01.2015).

Depth distributions of $^{137}Cs/^{239+240}Pu$ and $^{241}Am/^{239+240}Pu$ ratios in sediment outside Sellafield are relatively even down through the sediment core (*Fig. 25*). The $^{137}Cs/^{239+240}Pu$ ratio varied between 0.5 and 0.9 while the $^{241}Am/^{239+240}Pu$ ratio ranged between 2.5 and 3.3. For the ^{137}Cs results it would be somewhat higher if it was adjusted for decay (see chapter 2.1.). If it is assumed that the release time was 60 year ago, a mean $^{137}Cs/^{239+240}Pu$ ratio would be 2.8. Checking the $^{137}Cs/^{239+240}Pu$ ratio for integrated Sellafield releases between 1952 -1998 was approximately 67, and for $^{241}Am/^{239+240}Pu$ it was approximately 0.9 (Vintró et al. 2000)
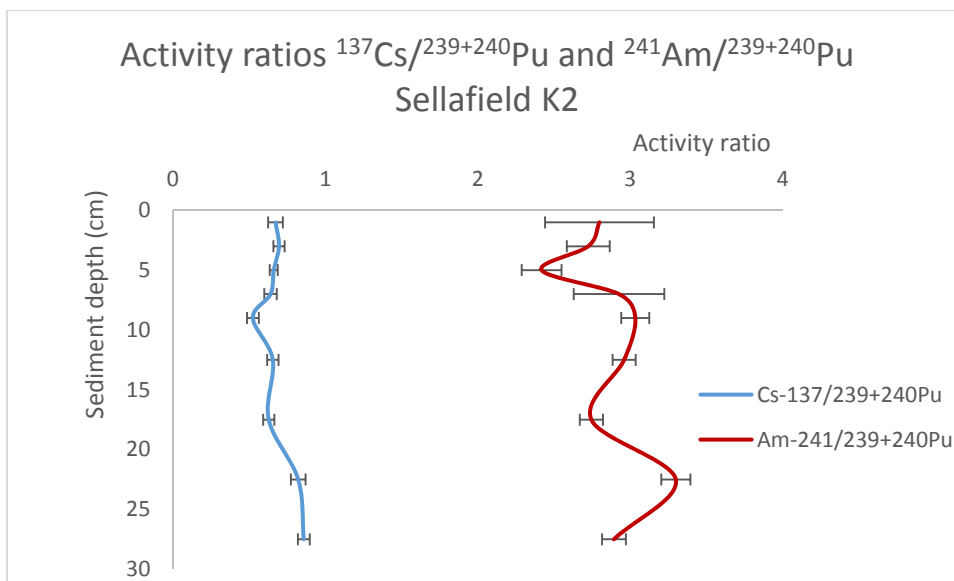
Figure 25. Depth distributions of $^{137}Cs/^{239+240}Pu$ and $^{241}Am/^{239+240}Pu$ activity concentrations from Sellafield K2 (ref.date 01.01.2015).

Isotopic ratios

The $^{240}Pu/^{239}Pu$ isotopic ratio at SRS showed a surprisingly even distribution, where the upper layer having a ratio of 0.11±0.007 and the lower layer having a Pu ratio of 0.08±0.007 (*Fig. 26*). In order to test the presence of significantly different ratios, different statistical approaches was applied. The distribution was divided into two parts, 0-7 cm and 8-18 cm. The transition point was excluded. Mean and propagated uncertainty including measurement uncertainties resulted in the upper layer having a ratio of 0.11±0.007 and the lower layer having a ratio of 0.08±0.007. Mean and sample standard deviation resulted in the upper layer having a ratio of 0.11±0.009 and the lower layer having a ratio of 0.08±0.009. Applying weighted mean and standard deviation based on $^{239+240}Pu$ activity resulted in the upper layer having a ratio of

0.116±0.009 and the lower layer having a ratio of 0.081±0.005. Checking their 95 % confidence interval for overlap by introducing 2 sigma provided significant result for application of mean with propagated standard deviation and for weighted mean and standard deviation, but not for mean and sample standard deviation. Introducing the two sided t-test provided a p-value= $4.9*10^{-6} \leq \alpha =0.05$, and stated that the sediment distribution belongs to two different means.

This change in ratio indicates some minor change in production and/or contribution from different sources. The contribution to the sediment seems to reflect the production from weapons grade Pu when compared to global fallout. The high uncertainties (5-80 %) relates to the low levels of ^{240}Pu. The change in ratios indicate a change in R-reactors production somewhere between 1961 -1964. SRS reactors were initially operated with 6% ^{240}Pu (providing a Pu isotope ratio of 0.06), but it is possible that R.reactor was re-tasked for some specific purpose that is not common knowledge (pers. comm. John Pinder).

Figure 26. Depth distribution of $^{240}Pu/^{239}Pu$ isotopic ratios SRS A9, including trend lines of mean isotopic ratio, weapons signature from SRS and global fallout range (GF).

The depth distribution of isotopic ratios from Sellafield (K2) vary between 0.20 and 0.22, and increases by depth (*Fig. 27*). The presence of significantly different ratios was tested as for Savannah River Site. The distribution was divided into two parts, 0-20 cm and 20-30 cm. Mean

and propagated uncertainty including measurement uncertainties resulted in the upper layer having a Pu ratio of 0.21±0.003 and the lower layer having a ratio of 0.22±0.001. Mean and sample standard deviation resulted in the upper layer having a ratio of 0.21±0.001 and the lower layer having a ratio of 0.22±0.002. Applying weighted mean and standard deviation based on $^{239+240}$Pu activity resulted in the upper layer having a ratio of 0.21±0.003 and the lower layer having a ratio of 0.224±0.0003. Checking their 95 % confidence interval for overlap by introducing 2 sigma provided significant result for all approaches. Introducing two sided t-test provided a p-value = 0.003 ≤ α =0.05, stating that the sediment distribution belongs to two different means.

The relative even distribution in the sediment layer can be explained by tidal and wave mixing, bioturbation caused by benthic organisms, and trawling (Kershaw et al. 1999; Vintró et al. 2000) A trend line shows the mean ratio between 0-20 cm. The distribution does not provide information about historical sources, but indicates influence by more modern sources such as nuclear power production. This corresponds with findings from (Kershaw et al. 1995), which suggest that weapons grade signatures occur as deep as 1 m, and that the isotopic ratio between 0.2-0.22 persists until 60 cm sediment depth. The top layers are in addition to mixing, reflecting the decrease of Sellafield derived discharges since the early 1980s, as well as remobilization.

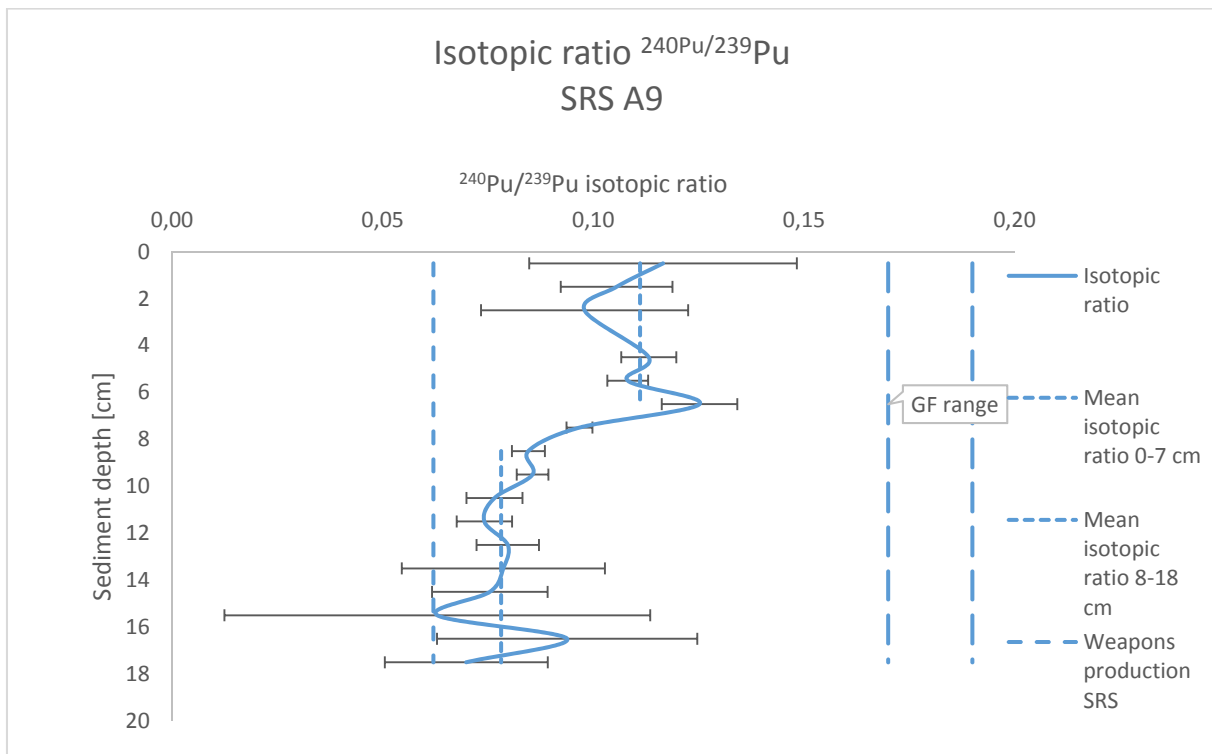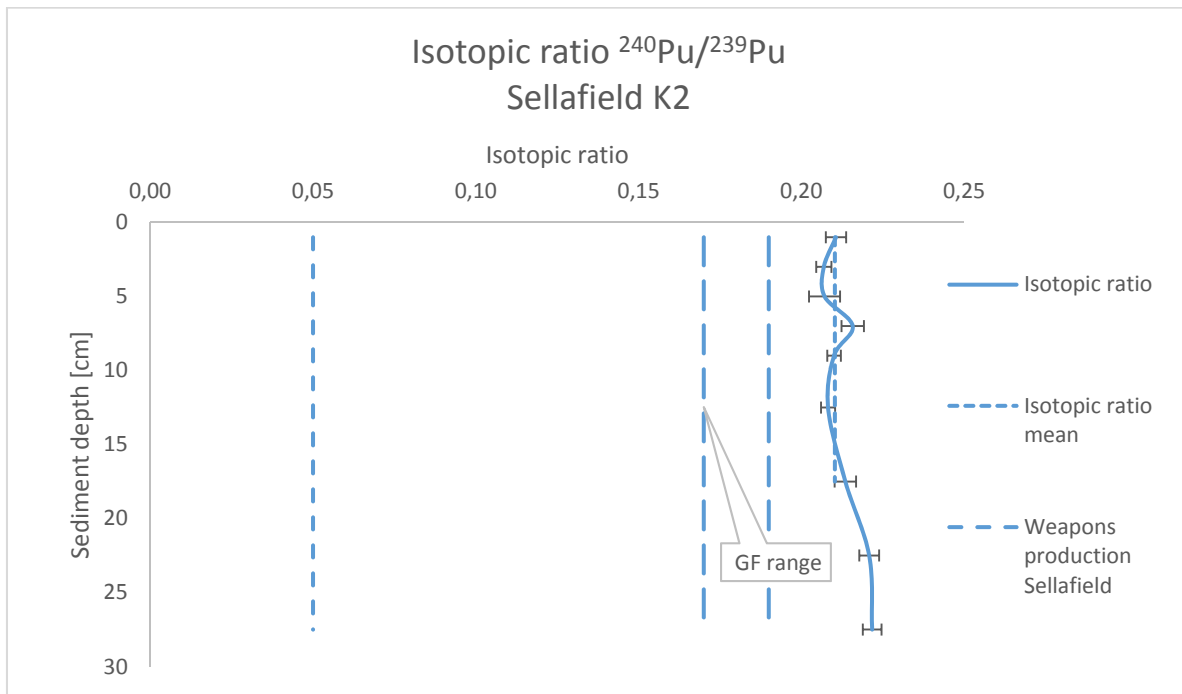*Figure 27. Depth distribution of ^{240}Pu/^{239}Pu isotopic ratios Sellafield K2, including trend lines of mean isotopic ratio, weapons production signature Sellafield and global fallout range (GF).*

Combining ^{240}Pu/^{239}Pu isotopic ratio and ^{238}Pu/$^{239+240}$Pu activity ratio enables the differentiation between sources that otherwise would be difficult to separate. Combination of the Pu isotopic ratio and the ^{238}Pu/$^{239+240}$Pu activity ratio for some selected samples from SRS, Sellafield (K2) and Mayak PA illustrates that the differentiation of sources can be provided with higher resolution than if isotopic or activity ratio was applied separately (*figure 28*).

The soil sample originating from Mayak (3516) shows a clear weapons grade signature, 0.22 and 0.001 for ^{240}Pu/^{239}Pu isotopic and ^{238}Pu/$^{239+240}$Pu activity ratio, respectively. The samples from SRS are placed below the global fallout signature, and show a clear contribution from weapons grade production, and as expected, the deepest sediment layer (17-18 cm) showed a clearer contribution than the middle layer (6-7 cm). This is confirmed by looking at the ^{238}Pu/$^{239+240}$Pu activity ratio, which indicates weapons grade Pu with ratios below 0.1. The Mayak sediment sample has the highest ^{238}Pu/$^{239+240}$Pu activity ratio of almost 1.2, in correspondence with the work of Skipperud et al. (2005). The ^{240}Pu/^{239}Pu isotopic ratio of 0.12, less than global fallout, indicates an influence from other sources, probably reprocessing of civil fuel.

The ^{240}Pu/^{239}Pu isotope ratios and the ^{238}Pu/$^{239+240}$Pu activity ratios in the Sellafield K2 samples almost overlap, and no significant difference could be seen for any of the ratios. An isotopic ratio of over 0.2 and a corresponding ^{238}Pu/$^{239+240}$Pu activity ratio of 0.2 indicates the presence of a civil source such as reprocessing of civil reactor waste.
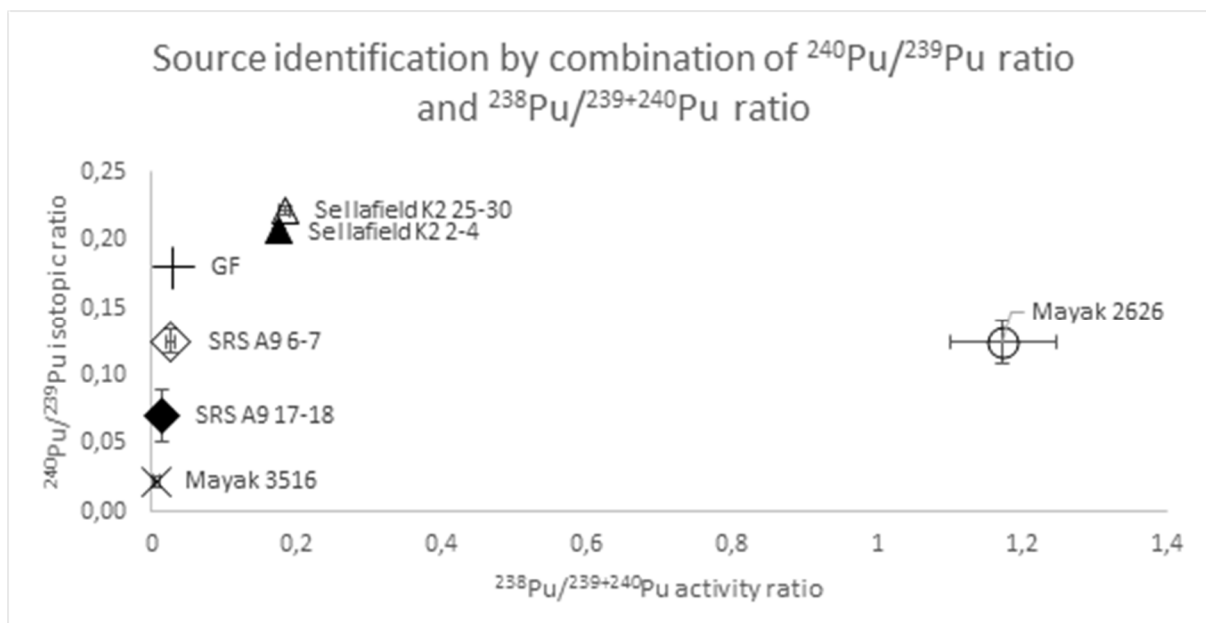
Figure 28. Combination of $^{240}Pu/^{239}Pu$ isotopic ratio and $^{238}Pu/^{239+240}Pu$ activity ratio for selected samples from Sellafield, SRS, and Mayak PA from a combination of ICP_MS and alpha-spectrometry (1σ). X: Mayak 3516, circle: Mayak 2626, black diamond: SRS 17-18, diamond: SRS 6-7, black triangle: Sellafield K2 2-4, triangle: Sellafield K2 25-30, cross: global fallout (ref.date 01.01.2015).

The present work demonstrates that Pu isotope ratios and $^{238}Pu/^{239+240}Pu$ activity ratios can be a powerful tool to distinguish between contaminated sites and releasing sources. For the samples investigated, the signature of most sample cores are unique and significantly different from each other. For SRS, surface and deeper layers also carried different signatures. In contrast, the Sellafield K2 samples were quite similar, as expected, since the core was not sufficiently deep to reflect the releases from weapon grade material production.

4. Conclusion

Particle identification

Heterogeneities (hotspots) were identified at Savannah River Site (Pond A) and Sellafield (K2 and Ravenglass) sediments. Uranium particles were identified at Sellafield (Ravenglass). It can not be concluded that these particles originate from Sellafield discharges, as uranium also occur naturally. Even so, it is very likely that the source of the particles identified are the Sellafield discharges.

Activity ratios

The activity ratios for cesium, americium and plutonium were determined for Savannah River Site (Pond A) and Sellafield (K2). For Savannah River site, the contamination is characterized by a high $^{137}Cs/^{239+240}Pu$ activity ratio ranging from 100-600, compared to the $^{137}Cs/^{239+240}Pu$ global fallout ratio (between 28 and 37). For Sellafield (K2), the contamination is characterized by a low $^{137}Cs/^{239+240}Pu$ activity ratio ranging from 0.5-0.9, and a high $^{241}Am/^{239+240}Pu$ ratio ranging from 2.5-3.3, compared to the $^{241}Am/^{239+240}Pu$ global fallout ratio (0.36).

The vertical sediment profile of the $^{137}Cs/^{239+240}Pu$ activity ratios showed great variations for Savannah River Site, probably influenced by a release event in 1964. The vertical sediment profile of the $^{137}Cs/^{239+240}Pu$ and the $^{241}Am/^{239+240}Pu$ activity ratios were relative evenly distributed down the core for Sellafield (K2).

Isotope ratios

The plutonium isotope ratio was determined for Savannah River Site (Pond A) and Sellafield (K2). The contaminated sediment from Savannah River Site can be characterized by a low $^{240}Pu/^{239}Pu$ isotope ratio, ranging from 0.06-0.12, compared to the $^{240}Pu/^{239}Pu$ global fallout ratio of 0.18. Sellafield contaminated sediment can be characterized by a high $^{240}Pu/^{239}Pu$ isotope ratio, ranging from 0.2 to 0.22, compared to the global fallout Pu ratio.

It was observed a radionuclide composition that varied by depth for both Savannah River Site and Sellafield (K2). For Savannah River Site, the mean $^{240}Pu/^{239}Pu$ isotope ratio was 0.11±0.007 for the upper layers and 0.08±0.007 for the deeper layers. The changes in ratio indicate a change in production or contribution from other sources, and reflects the production of weapons grade Pu when compared to global fallout.

For Sellafield (K2), the mean $^{240}Pu/^{239}Pu$ isotope ratio was 0.21±0.001 for the upper layers and 0.22±0.002 for the deeper layers. The distribution do no provide information about

historical sources, but indicate influence from more modern sources such as nuclear power production or waste reprocessing. The even distribution down the core can be explained by tidal and wave mixing, bioturbation by benthic organisms, decrease of Sellafield derived discharges since the early 1980s, and remobilization.

Combining the $^{240}Pu/^{239}Pu$ isotope ratio and the $^{238}Pu/^{239+240}Pu$ activity ratio enabled to differentiate between contaminated sediment from the three reprocessing power plants at Savannah River Site, Sellafield and Mayak PA. For the samples investigated, the signature of the sample cores were unique and significantly different from each other. For SRS, different signatures could also be observed in the surface layers compared to the deeper layers. Hence, differentiation between the source term and the releases associated with specific production sites, and in some cases also changes in production and releases over time (different sediment depths) could be obtained using the present choice of radionuclide ratios determined in contaminated sediments downstreams from the point of release.

5. References

Abraham, J., Whicker, F., Hinton, T. & Rowan, D. (2000). Inventory and spatial pattern of 137Cs in a pond: a comparison of two survey methods. *Journal of environmental radioactivity*, 51 (2): 157-171.

Balcaen, L., Woods, G., Resano, M. & Vanhaecke, F. (2013). Accurate determination of S in organic matrices using isotope dilution ICP-MS/MS. *Journal of Analytical Atomic Spectrometry*, 28 (1): 33-39.

Buesseler, K. O. (1997). The isotopic signature of fallout plutonium in the North Pacific. *Journal of Environmental Radioactivity*, 36 (1): 69-83.

Bunzl, K. (1998). Detection of radioactive hot particles in environmental samples by repeated mixing. *Applied radiation and isotopes*, 49 (12): 1625-1631.

Bunzl, K. & Tschiersch, J. (2001). Detection of radioactive hot particles in environmental samples using a Marinelli-beaker measuring geometry. *Radiochimica Acta International journal for chemical aspects of nuclear science and technology*, 89 (9/2001): 599.

Cagno, S., Hellemans, K., Lind, O., Skipperud, L., Janssens, K. & Salbu, B. (2014). LA-ICP-MS for Pu source identification at Mayak PA, the Urals, Russia. *Environmental Science: Processes & Impacts*, 16 (2): 306-312.

Carlton, W. H., Murphy, C. E., Jr. & Evans, A. G. (1994). Radiocesium in the Savannah River Site environment. *Health Phys*, 67 (3): 233-44.

Christensen, G. C., Romanov, G., Strand, P., Salbu, B., Malyshev, S., Bergan, T., Oughton, D., Drozhko, E., Glagolenko, Y. & Amundsen, I. (1997). Radioactive contamination in the environment of the nuclear enterprise 'Mayak'PA. Results from the joint Russian-Norwegian field work in 1994. *Science of the total environment*, 202 (1): 237-248.

Clacher, A. P. (1995). *Development and application of analytical methods for environmental radioactivity*: University of Manchester.

Cook, G., MacKenzie, A., McDonald, P. & Jones, S. (1997). Remobilization of Sellafield-derived radionuclides and transport from the north-east Irish Sea. *Journal of Environmental Radioactivity*, 35 (3): 227-241.

Dai, M., Kelley, J. M. & Buesseler, K. O. (2002). Sources and migration of plutonium in groundwater at the Savannah River Site. *Environmental science & technology*, 36 (17): 3690-3699.

Dai, M., Buesseler, K. O. & Pike, S. M. (2005). Plutonium in groundwater at the 100K-Area of the US DOE Hanford Site. *Journal of Contaminant Hydrology*, 76 (3): 167-189.

Gaidar, O. (2011). Derivation of the source term and analysis of the radiological consequences for the design basis accidents at research reactor.

Godoy, M. L. D. P., Godoy, J. M., Roldão, L. A. & Tauhata, L. (2009). Determination of total content and isotopic compositions of plutonium and uranium in environmental samples for safeguards purposes by ICP-QMS. *Journal of environmental radioactivity*, 100 (8): 613-625.

Goodge, J. *Energy-Dispersive X-Ray Spectroscopy (EDS)*. http://serc.carleton.edu/research_education/geochemsheets/eds.html: University of Minnesota (accessed: 26. april).

Gouzy, A. (2004). Etude du comportement du plutonium au cours de la diagenèse précoce des sédiments marins: applications à deux environnements marins marqués par les rejets issus d'usines de retraitement de combustibles usés.

Gray, J., Jones, S. & Smith, A. (1995). Discharges to the environment from the Sellafield site, 1951-1992. *Journal of Radiological Protection*, 15 (2): 99.

Grubbs, F. E. (1969). Procedures for detecting outlying observations in samples. *Technometrics*, 11 (1): 1-21.

Halverson, N. (1998). Sampling and Analysis of Pond 2, Pond 5, and the P-Reactor Canal Sediments: Savannah River Site, Aiken, SC (US).

Hinton, T. & Pinder III, J. (2001). A review of plutonium releases from the Savannah River Site, subsequent behavior within terrestrial and aquatic environments and resulting dose to humans. *Radioactivity in the Environment*, 1: 413-435.

IAEA. (2011). Radioactive Particles in the Environment: Sources, Particle Characterization and Analytical Techniques. *IAEA-TECDOC-1663*.

Jaeschke, B., Lind, O. C., Bradshaw, C. & Salbu, B. (2014). Retention of radioactive particles and associated effects in the filter-feeding marine mollusc Mytilus edulis.

Jernström, J. (2006). Development of analytical techniques for studies on dispersion of actinides in the environment and characterization of environmental radioactive particles.

Kershaw, P., Woodhead, D., Lovett, M. & Leonard, K. (1995). Plutonium from European reprocessing operations—its behaviour in the marine environment. *Applied radiation and isotopes*, 46 (11): 1121-1134.

Kershaw, P., Denoon, D. & Woodhead, D. (1999). Observations on the redistribution of plutonium and americium in the Irish Sea sediments, 1978 to 1996: concentrations and inventories. *Journal of Environmental Radioactivity*, 44 (2): 191-221.

L'Annunziata, M. F. (2012). *Handbook of radioactivity analysis*: Academic Press.

Lee, M. & Clark, S. (2005). Activities of Pu and Am isotopes and isotopic ratios in a soil contaminated by weapons-grade plutonium. *Environmental science & technology*, 39 (15): 5512-5516.

Lilley, J. S. (2013). *Nuclear physics: principles and applications*: John Wiley & Sons.

Lind, O. C. (2006). *Characterisation of radioactive particles in the environment using advanced techniques*: Norwegian University of Life Sciences, Department of Plant and Environmental Sciences.

Ltd., S. (2014). Particles in the Environment Annual Report 2013-14.

Mocak, J., Bond, A., Mitchell, S. & Scollary, G. (1997). A statistical overview of standard (IUPAC and ACS) and new procedures for determining the limits of detection and quantification: application to voltammetric and stripping techniques (technical report). *Pure and Applied Chemistry*, 69 (2): 297-328.

Morris, K., Butterworth, J. C. & Livens, F. R. (2000). Evidence for the Remobilization of Sellafield Waste Radionuclides in an Intertidal Salt Marsh, West Cumbria, U.K. *Estuarine, Coastal and Shelf Science*, 51 (5): 613-625.

Nassef, M., El Mongy, S., Diab, A. & El-Tahawy, M. (2008). Determination of plutonium isotopes in standard IAEA reference materials by destructive analytical technique. *J Nucl Radiat Phys*, 3 (1): 21-30.

Neu, M. P., Goff, G. S. & Runde, W. (2011). Plutonium. *ChemInform*, 42 (30).

Newbury, D. E., Joy, D. C., Echlin, P., Fiori, C. E. & Goldstein, J. I. (2003). *Scanning electron microscopy and X-ray microanalysis*: Springer.

Ohno, T., Muramatsu, Y., Shikamori, Y., Toyama, C., Okabe, N. & Matsuzaki, H. (2013). Determination of ultratrace 129I in soil samples by Triple Quadrupole ICP-MS and its application to Fukushima soil samples. *Journal of Analytical Atomic Spectrometry*, 28 (8): 1283-1287.

Ohno, T. & Muramatsu, Y. (2014). Determination of radioactive cesium isotope ratios by triple quadrupole ICP-MS and its application to rainwater following the Fukushima Daiichi Nuclear Power Plant accident. *Journal of Analytical Atomic Spectrometry*, 29 (2): 347-351.

Oughton, D. H., Fifield, L. K., Day, J. P., Cresswell, R. C., Skipperud, L., Di Tada, M. L., Salbu, B., Strand, P., Drozcho, E. & Mokrov, Y. (2000). Plutonium from Mayak: Measurement of isotope ratios and activities using accelerator mass spectrometry. *Environmental science & technology*, 34 (10): 1938-1945.

Pentreath, R. J. (1985). Radioactive discharges from Sellafield (UK). In *Behaviour of Radionuclides Released into Coastal Waters*, pp. 67-110: IAEA Vienna.

Remotrans, E. (2004). project, November 2000-October 2003. *Processes regulating remobilisation, bioavailability and translocation of radionuclides in marine sediments, EU Fifth Framework Program, FP5-EURATOM*.

Runde, W. (2011). Americium and curium. *ChemInform*, 42 (30).

Sakaguchi, A., Kawai, K., Steier, P., Quinto, F., Mino, K., Tomita, J., Hoshi, M., Whitehead, N. & Yamamoto, M. (2009). First results on 236U levels in global fallout. *Science of The Total Environment*, 407 (14): 4238-4242.

Salbu, B. & Krekling, T. (1998). Characterisation of radioactive particles in the environment†. *Analyst*, 123 (5): 843-850.

Salbu, B. (2000). *Speciation of radionuclides in the environment*: Wiley Online Library.

Salbu, B., Lind, O. & Skipperud, L. (2004). Radionuclide speciation and its relevance in environmental impact assessments. *Journal of environmental radioactivity*, 74 (1): 233-242.

Salbu, B. (2009). Challenges in radioecology. *Journal of Environmental Radioactivity*, 100 (12): 1086-1091.

Skipperud, L. (2004). *Plutonium in the environment: sources and mobility*: Norwegian University of Life Sciences, Department of Plant and Environmental Sciences.

Skipperud, L., Salbu, B., Oughton, D. H., Drozcho, E., Mokrov, Y. & Strand, P. (2005). Plutonium contamination in soils and sediments at Mayak PA, Russia. *Health Physics*, 89 (3): 255-266.

Tanner, S. D., Li, C., Vais, V., Baranov, V. I. & Bandura, D. R. (2004). Chemical resolution of Pu+ from U+ and Am+ using a band-pass reaction cell inductively coupled plasma mass spectrometer. *Analytical chemistry*, 76 (11): 3042-3048.

Tvedt & Tjelmeland. (2014). *The Cold War*. www.snl.no. Available at: https://snl.no/Den_kalde_krigen (accessed: 28. april).

U.S.E.P.A. (2012). *Savannah River Site (USDOE)*. Available at: http://www.epa.gov/region4/superfund/sites/fedfacs/savrivsc.html.

Vandenhove, H., Hurtgen, C. & Payne, T. (2010). Radionuclides in the environment: uranium. In: Radionuclides in the Environment, West Sussex, United Kingdom, John Wiley & Sons, Ltd.

Vintró, L. L., Smith, K. J., Lucey, J. A. & Mitchell, P. I. (2000). *The environmental impact of the Sellafield discharges*. SCOPE-RADSITE Workshop Proceedings, Brussels. 27 pp.

Wakeford, R. (2007). The Windscale reactor accident—50 years on. *Journal of Radiological Protection*, 27 (3): 211.

Webb, G., Anderson, R. & Gaffney, M. (2006). Classification of events with an off-site radiological impact at the Sellafield site between 1950 and 2000, using the International Nuclear Event Scale. *Journal of Radiological Protection*, 26 (1): 33.

Wendel, C. C. (2007). Determination of iodine-129 in Laminaria hyperborea.

Wendel, C. C. (2014). Source identification of Pu and 236U deposited on Norwegian territories.

Whicker, F. W., Pinder III, J. E., Bowling, J. W., Alberts, J. J. & Brisbin, I. L., Jr. (1990). Distribution of Long-Lived Radionuclides in an Abandoned Reactor Cooling Reservoir. *Ecological Monographs*, 60 (4): 471-496.

Wood, M. D., Beresford, N. A., Copplestone, D., Wood, M., Beresford, N. & Copplestone, D. (2011). Limit of detection values in data analysis: Do they matter? *Radioprotection*, 46 (06): S85-S90.

Zeghnoun, A., Pascal, M., Fréry, N., Sarter, H., Falq, G., Focant, J.-F. & Eppe, G. (2007). Dealing with the non-detected and non-quantified data. The example of the serum dioxin data in the French dioxin and incinerators study. *Organohalogen Compounds*, 69: 2288-2291.

Zeissler, C. J., Wight, S. A. & Lindstrom, R. M. (1998). Detection and characterization of radioactive particles. *Applied radiation and isotopes*, 49 (9): 1091-1097.

Zheng, J., Tagami, K., Watanabe, Y., Uchida, S., Aono, T., Ishii, N., Yoshida, S., Kubota, Y., Fuma, S. & Ihara, S. (2012). Isotopic evidence of plutonium release into the environment from the Fukushima DNPP accident. *Scientific reports*, 2.

Appendix A

LOI (Loss on Ignition) was determined for all sediment depths for both Savannah River Site (Pond A, core A9) and Sellafield K2. Results of calculations are shown below.

Calculated LOI SRS A9.

Sample	Pre-ignition weight (g)	Post-ignition weight (g)	LOI %
SRS A9 0-1	1.08	0.43	60.3 %
SRS A9 1-2	1.23	0.47	62.2 %
SRS A9 2-3	0.04	0.01	69.9 %
SRS A9 4-5	1.14	0.85	24.9 %
SRS A9 5-6	1.12	1.00	11.2 %
SRS A9 6-7	0.97	0.90	7.2 %
SRS A9 7-8	1.02	0.95	7.2 %
SRS A9 8-9	1.01	0.94	6.9 %
SRS A9 9-10	1.10	1.03	6.8 %
SRS A9 10-11	1.03	0.95	7.5 %
SRS A9 11-12	1.32	1.23	6.9 %
SRS A9 12-13	1.07	1.01	6.4 %
SRS A9 13-14	1.18	1.12	4.8 %
SRS A9 14-15	1.06	1.01	4.9 %
SRS A9 15-16	1.16	1.11	4.7 %
SRS A9 16-17	1.05	1.02	3.3 %
SRS A9 17-18	1.04	1.00	4.2 %

Calculated LOI Sellafield K2

Sample	Pre-ignition weight (g)	Post-ignition weight (g)	LOI %
Sellafield K2 0-2	1.00	0.93	7.3 %
Sellafield K2 2-4	1.11	1.04	6.0 %
Sellafield K2 4-6	1.09	1.03	6.1 %
Sellafield K2 6-8	1.08	1.03	4.5 %
Sellafield K2 8-10	1.16	1.11	4.8 %
Sellafield K2 10-15	1.36	1.32	3.2 %
Sellafield K2 15-20	1.10	1.06	3.6 %
Sellafield K2 20-25	1.08	1.04	3.6 %
Sellafield K2 25-30	1.23	1.19	3.3 %

Appendix B

The raw data from gamma measurements of A9 and K2 in Ge-detectors are listed below. The numbers was subsequently adjusted for background, and updated with correction factors before calculating activity concentrations. The [241]Am levels in the Savannah River Site Core were low, near or below detection limit, and was not included in the dataset.

Raw data Ge-measurements of K2 and A9.

Sediment core/depth	time (s)	weight (g)	volume	Am-241 Net area (counts)	counting uncertainty	Cs-137 Net area (counts)	counting uncertainty
K2 0-2	14782	10.51	15 ml	720	89	737	34
K2 2-4	7952	21.15	20 ml	3941	192	827	35
K2 4-6	69999	20.85	20 ml	4300	212	4247	83
K2 6-8	10252	21.80	20 ml	849	84	664	31
K2 8-10	5493	22.68	20 ml	3730	65	531	34
K2 10-15	5550	25.84	20 ml	3965	68	718	33
K2 15-20	4799	24.76	20 ml	3810	67	712	34
K2 20-25	3317	23.03	20 ml	2940	59	596	29
K2 25-30	5428	22.42	20ml	6313	85	1517	44
A9 0-1	419784	2.28	10 ml	102	167	47166	251
A9 1-2	2764	2.83	10 ml	3	13	478	24
A9 2-3	58458	1.12	5ml	5	55	7498	106
A9 3-4	58290	8.69	10 ml	19	67	15508	132
A9 4-5	83096	7.31	10 ml	247	94	64201	260
A9 5-6	250030	16.74	20 ml	498	190	285977	546
A9 6-7	249893	22.61	20 ml	7703	210	798519	913
A9 7-8	92983	21.59	20 ml	211	137	231783	488
A9 8-9	249527	17.07	15 ml	620	211	513347	727
A9 9-10	340557	23.73	20ml	4090	227	1025936	1035
A9 10-11	340326	24.72	20 ml	1431	218	285201	549
A9 11-12	91763	24.50	20 ml	143	100	54085	241
A9 12-13	1565	19.34	15 ml	15	11	448	22
A9 13-14	1111940	26.19	20 ml	211	333	426385	721
A9 14-15	3885	23.21	20 ml	20	16	929	36
A9 15-16	1111146	24.51	15 ml	455	285	101140	379
A9 16-17	9592	23.37	15 ml	36	26	723	32
A9 17-18	4661	23.51	15 ml	22	17	1232	39

Appendix C

It became necessary to introduce correction factors for quality assurance. The factors were based on measurements of standard calibration solutions and certified reference material with different geometries.

Correction factors Ge-detectors for measurements of ^{137}Cs and ^{241}Am.

		Correction factors (cps/Bq)					
		Stanadard calibration solution				CRM	
		^{241}Am	sigma	^{137}Cs	sigma	^{241}Am	^{137}Cs
Detektor 1	5 ml	0.0856	0.0010	0.0446	0.0012	0.73	1
	10 ml	0.0704	0.0008	0.0382	0.0011	0.68	0.92
	15 ml	0.0584	0.0010	0.0320	0.0013	0.61	0.88
	20 ml	0.0463	0.0006	0.0258	0.0007		
Detektor 2	5 ml	0.0076	0.0001	0.0244	0.0007	1	1.03
	10 ml	0.0069	0.0001	0.0208	0.0008	0.92	0.98
	15 ml	0.0062	0.0001	0.0171	0.0007	0.75	0.92
	20 ml	0.0055	0.0001	0.0134	0.0004		

Calculated background levels for Ge-detectors are listed below.

Background levels Ge-detectors.

	Background Ge-detectors				
Detector	Isotope	time (s)	net area	cps	sigma
1	^{241}Am	413443	0	0	0
	^{137}Cs	413443	973	2.4E-03	4.1E-04
2	^{241}Am	259299	141	5.4E-04	5.0E-04
	^{137}Cs	259299	2721	1.0E-02	4.0E-08

Appendix D

Raw data from alpha spectrometry are listed below. The numbers were subsequently adjusted for background and losses. The added ^{242}Pu tracer had activity 0.00370 ± 0.00003 Bq.

Raw data from alpha spectrometry.

Sample	t (s)	mass(g)	^{242}Pu Gross area	counting uncertainty	^{238}Pu Gross area	counting unc.	$^{239+240}$Pu Gross area	counting unc.
Mayak 2626	247515	1.2471	107	10	567	24	482	22
Mayak 3516	247568	1.2554	52	7	5	2	447	21
SRS A9 6-7	171364	5.1184	9	3	16	4	572	24
SRS A9 17-18	171497	5.0136	74	9	3	2	114	11
Sellafield K2 2-4	85787	3.0148	38	6	1446	38	8224	91
Sellafield K2 25-30	247875	3.0306	10	3	711	27	3860	62
IAEA 384	88989	1.0754	12	3	97	10	322	18

Background levels alpha-spectrometer.

Background alpha-spectrometer

	Detector	t (s)	gross area	cps	sigma
^{242}Pu	2	1207862	7	5.8E-06	2.2E-06
	3	1207896	2	1.7E-06	1.2E-06
	4	1207922	2	1.7E-06	1.2E-06
$^{239+240}$Pu	2	1207862	3	2.5E-06	1.4E-06
	3	1207896	0	0	0
	4	1207922	5	4.1E-06	1.9E-06
^{238}Pu	2	1207862	7	5.8E-06	2.2E-06
	3	1207896	6	5.0E-06	2.0E-06
	4	1207922	10	8.3E-06	2.6E-06

Appendix E

Software settings for ICP-MS measurements of Pu are listed below.

Software settings for ICP-MS triple quadrupole.

Software parameters	
Peak pattern	3 points
Replicates	3
Sweeps per replicate	1000
Tune mode	CO_2
Isotopes	^{254}U, ^{239}Pu, ^{240}Pu, ^{242}Pu
Integration time	0.51 s (^{238}U), 9 s ($^{239, 240, 242}Pu$)
Sample introduction	ISIS discrete sampling
Stabilize	50 s
Loop Wash	40 s
Wash solution	0.8M HNO_3 + 0.006M HF

Hardware for ICP-MS instrument are listed below.

Hardware description ICP-MS triple quadrupole.

Hardware parameters	
Lense	S-lense
Nebulizer	Concentric quarts
Spray chamber	Scott double pass, quarts
Injector	Quarts
Torch	Quarts
Cones	Platinum
Tubes	Teflon
Loop	200 cm, 1.0 mL

Appendix F

The instrumental settings for ICP-MS measurements of Pu are listed below.

Instrumental settings for ICP-MS triple quadrupole.

Instrumental parameters	
Plasma conditions	
RF Power	1500 W
Sampling depth	7 mm
Carrier gas	0.7 L/min
Nebulizer pump	200 μL/min
Spray chamber temperature	2 ℃
Makeup gas	0.5 L/min
Loop size	1 ml
Cell conditions	
Cell gas	CO_2 32%
Octapole bias	-1 V
Octapole RF	200 V
Energy discrimination	8 mV
4th cell gas flow rate	0.32 mL/min CO_2
Lenses	
Extract 1	4.2 V
Extract 2	-245 V
Omega Bias	-195 V
Omega Lens	27.8 V
Cell Entrance	-48 V
Cell Exit	-56 V
Deflect	5.2 V
Plate Bias	-35 V

Appendix G

Raw data from ICP-MS measurements of samples from Savannah River Site A9 are listed below.

Raw data ICP-MS measurements SRS A9

| Sample Name	Comment	238 -> 254 U [CO2 32%] Conc. [ppt]	CPS	CPS RSD	239 -> 239 Pu [CO2 32%] CPS	CPS RSD	240 -> 240 Pu [CO2 32%] CPS	CPS RSD	242 -> 242 Pu [CO2 32%] Conc. [ppq]	CPS	CPS RSD
wash			159.656	19.162226	0.066	223.606798	0.022	223.606798		0.044	223.606798
cal blank		0.05236228	193.782	24.3288746	0.022	223.606798	0.022	223.606798	0.10730286	0.044	136.930639
cal blank		0.02027316	186.33	16.3911733	0.066	149.071198	0.022	223.606798	-0.10730286	0	0 N/A
cal blank		0	181.622	11.5453538	0.066	91.2870929	0.022	223.606798	0	0.022	223.606798
std1		0.07262682	198.488	12.3120239	0.132	108.653373	0.066	149.071198	9.51337373	1.9725	16.0177919
std2		0.36656177	266.748	10.9818326	0.022	223.606798	0 N/A	0 N/A	92.0365867	18.892	5.21557991
std3		2.73650596	817.116	4.24173797	0.066	91.2870929	0.066	149.071198	437.678598	89.758	2.3782645
std4		12.6512944	3119.61	2.56732315	0.022	223.606798	0.044	136.930639	2356.5073	483.17	1.80171256
Std U 1000 ppt		1000	232409.876	1.37645877	0.088	104.582503	0 N/A	0 N/A	3.25810492	0.69	36.7070294
wash		0.12669432	211.044	13.605712	0.11	100	0.022	223.606798	1.39493714	0.308	46.5657315
4	SRS A9 0-1	154.826751	36136.768	0.91536316	24.356	10.2262635	2.914	24.0680018	1713.42177	351.32	1.68379279
5	SRS A9 1-2	165.923239	38713.686	0.89525113	26.822	4.72907353	2.91	10.9508284	1789.94822	367.01	2.01780935
6	SRS A9 2-3	105.573433	24698.756	0.52397613	21.178	4.32888615	2.156	23.1832083	1840.02939	377.278	2.50016354
8	SRS A9 3-4	37.9916931	8999.722	3.47249272	2.466	23.2572665	0.22	61.2372436	1826.91893	374.59	1.28213215
9	SRS A9 4-5	1039.8972	241675.132	0.50801353	354.652	1.95190047	40.202	5.42011637	1777.69618	364.498	1.75742641
11	SRS A9 5-6	455.425015	105944.178	0.52447699	816.766	1.43433339	88.422	4.24709404	1680.36274	344.542	1.71932015
12	SRS A9 6-7	2134.21416	495806.45	0.38767985	895.838	1.4186365	112.224	7.02200905	1445.91575	296.474	2.34767514
13	SRS A9 7-8	968.975773	225205.174	1.0445973	632.576	0.74760639	61.246	3.09632115	1595.37887	327.118	3.09894886
14	Referansem	245.545101	57204.132	0.39975467	8.756	10.3503036	1.354	13.5539967	1824.96797	374.19	3.53841841
std 4		11.0040529	2737.074	2.26781062	0.466	62.0576223	0.11	100	2200.84988	451.256	2.32850695
14	Referansem	239.747124	55857.678	1.73916582	7.888	8.04466077	1.778	17.7473084	1801.00041	369.276	3.23696121
15	SRS A9 8-9	1994.31881	463318.798	0.33405721	506.924	2.36943271	42.956	3.95892763	1275.95778	261.628	2.07416223
16	SRS A9 9-10	1309.11631	304195.418	0.86158838	412.48	2.23687839	35.38	3.75248577	1301.43733	266.852	3.53155043
17	SRS A9 10-11	283.789396	66085.538	1.40354237	334.83	1.79589831	25.712	8.46296912	1502.81553	308.14	2.25663769
19	SRS A9 11-12	313.917996	73082.25	1.00649728	390.944	1.86908982	29.066	8.6449581	1654.79539	339.3	2.3933974
20	SRS A9 12-13	152.99842	35712.178	1.13752132	118.244	3.05510853	9.512	8.64674057	1523.21283	312.322	1.65341633
21	SRS A9 13-14	342.62669	79749.22	0.35608181	51.158	5.55399905	4.112	29.250388	1585.63382	325.12	1.9116161
22	Referansem	239.669769	55839.714	0.63250654	67.822	2.73102207	4.068	9.96924805	1829.18204	375.054	3.57070937
23	SRS A9 14-15	486.52937	113167.488	0.58018897	23.556	8.53009065	1.868	14.6626227	1619.56104	332.076	2.89437222
24	SRS A9 15-16	291.832474	67953.368	1.85611015	9.468	13.3229391	0.6925	64.809237	1606.01161	329.298	1.99036294
25	SRS A9 16-17	316.803381	73752.318	1.54159361	10	6.52495211	1.022	27.8598767	1820.40272	373.254	2.67460353
26	SRS A9 17-18	337.730033	78612.078	1.03308197	32.714	4.38416271	2.378	25.8653167	1864.63101	382.322	2.36848302
std 4		9.5867663	2407.94	1.09546385	0.112	223.606798	0 N/A	0 N/A	1973.01665	404.544	1.72928323

Appendix H

Raw data from ICP-MS measurements of Sellafield K2 samples are listed below.

Raw data ICP-MS measurements Sellafield K2

Sample Nam	Comment	238 -> 254 U [CO2 32%] Conc. [ppt]	CPS	CPS RSD	239 -> 239 Pu [CO2 32%] CPS	CPS RSD	240 -> 240 Pu [CO2 32%] CPS	CPS RSD	242 -> 242 Pu [CO2 32%] Conc. [ppq]	CPS	CPS RSD
28	Sellafield K2 0-2	177.935	41503.082	0.389	3782.056	0.952	796.676	1.127	1799.381	368.944	1.684
29	Sellafield K2 2-4	165.14	38531.02	0.87	3285.958	0.570	679.934	0.979	1786.261	366.254	1.360
30	Sellafield K2 4-6	160.47	37447.59	1.16	2031.966	0.761	420.902	2.169	1130.289	231.762	1.351
31	Referansematerii	244.26	56906.67	1.14	263.496	2.033	14.112	8.250	785.379	161.046	2.682
33	Sellafield K2 6-8	70.73	16607.19	1.05	3698.434	0.543	798.074	1.497	1922.61	394.21	1.54
34	Sellafield K2 8-10	109.44	25596.76	0.71	3904.424	0.687	820.122	0.717	1854.876	380.322	2.833
35	Sellafield K2 10-1	78.194	18340.484	1.634	3721.662	0.933	774.872	0.453	1867.5	382.9	1.7
36	Referansematerii	225.222	52484.524	0.495	273.362	1.756	15	14	801.328	164.316	4.335
37	Mayak 2626 husst	11.557	2865.416	2.526	72.956	7.396	9.134	9.995	1579.7	323.9	1.7
38	Sellafield K2 15-2	95.248	22300.906	1.829	3769.854	0.952	804.942	1.203	1520.599	311.786	2.112
39	Sellafield K2 20-2	92.150	21581.478	1.121	4148.358	0.373	916.15	1.33	1659.439	340.252	2.075
std 4		8.082	2058.382	3.121	7.09	22.15	1.378	39.689	1821.476	373.474	4.295
40	Sellafield K2 25-3	55.910	13165.544	1.146	5968.732	0.791	1323.542	1.035	1585.29	325.05	2.57
41	Mayak 3516 husst	11.422	2834.032	2.132	162.026	3.163	3.69	17.00	1562.105	320.296	2.067
43	HF begerglass A9	7.21	1855.95	3.799	3.934	25.826	0.778	35.029	8.018	1.666	20.643
44	HF begerglass K2	6.451	1679.798	3.591	22.242	7.198	4.914	9.220	6.828	1.422	49.059
45	HF begerglass K2	10.57	2636.66	2.70	131.314	1.489	28.824	10.296	38.590	7.934	16.513
41	Mayak 3516 husst	9.237	2326.734	4.822	137.826	4.910	3.066	20.916	1390.323	285.076	3.042
wash	<0.000		129.452	16.493	1.046	35.749	0.044	223.607	1.512	0.332	63.196
1	Blank tilsatt trace	5.019	1347.118	3.469	0.732	48.889	0.222	94.509	1520.589	311.784	2.828
2	Blank tilsatt trace	4.346	1190.974	1.862	0.666	69.901	0.088	162.980	1513.98	310.43	2.21
3	Blank tilsatt trace	5.754	1517.758	3.307	0.286	43.853	0.044	136.931	1504.776	308.542	1.485
7	Blank m/tracer	2.747	819.476	8.970	1.046	45.907	0.176	94.786	1168.870	239.672	2.198
std 4		6.985	1803.762	3.411	0.376	92.563	0.11	100.00	1628.672	333.944	1.836
10	Blank m/tracer	4.694	1271.796	2.188	0.288	100.736	0.132	108.653	1122.48	230.16	0.97
18	Blank m/tracer	16.86	4097.45	2.118	9.866	12.789	1.156	42.080	1228.374	251.872	3.180
27	Blank m/tracer	4.640	1259.248	3.467	0.332	67.399	0	N/A	1319.201	270.494	2.143
32	Blank m/tracer	1.98	641.37	8.517	0.2	114.7	0.132	69.722	1208.435	247.784	2.768
42	Blank m/tracer	2.63	793.19	3.890	0.088	136.931	0.044	223.607	1275.19	261.47	1.79

Appendix I

Investigations of tracer showed that no significant contributions from analytes (^{239}Pu and ^{240}Pu) were present.
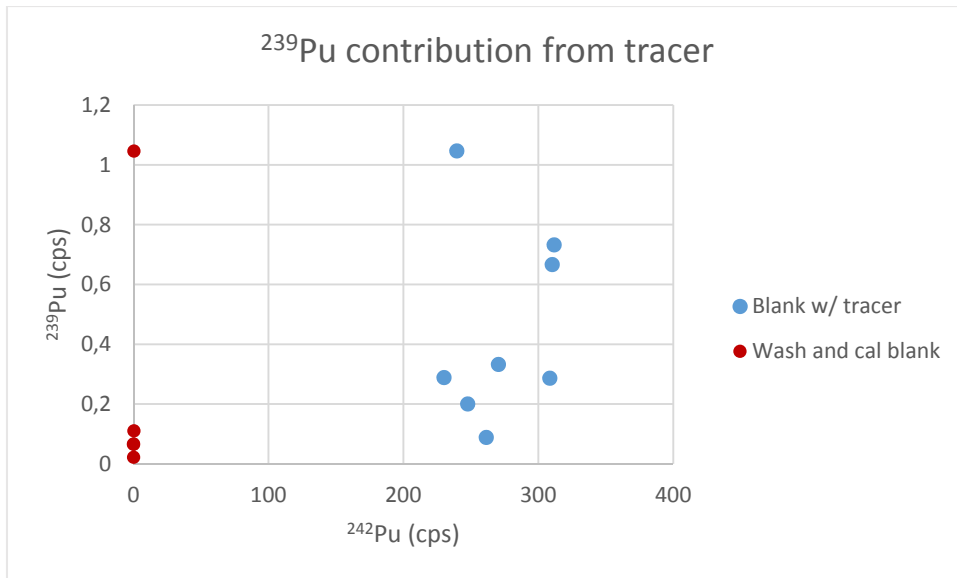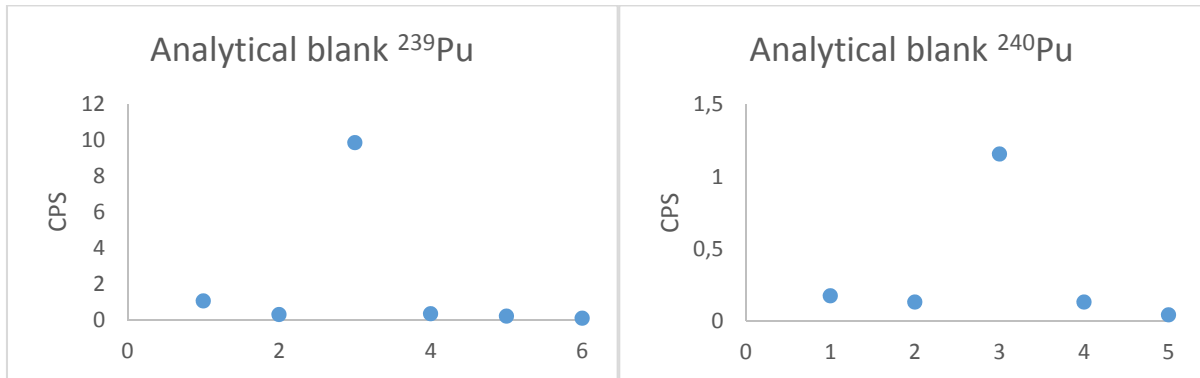

^{239}Pu contribution from tracer.
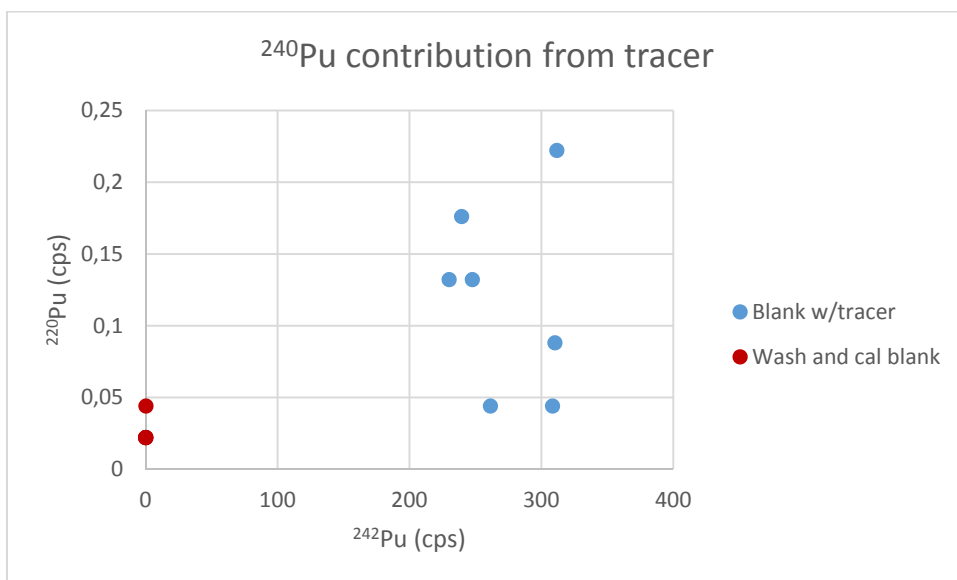
^{240}Pu contribution from tracer.

Appendix J

Suspicion of the presence of an outlier in the blank population was based on high cps from ICP-MS measurements for one blank.



Analytical blank signals of ICP-MS measurements

Calculations showed that $G_{calculated} \geq G_{tabulated}$, hence Grubbs's test rejected H_o and accepted H_1 that one outlier was present with a significance level $\alpha = 0.01$.

Grubb's test for outliers

| Grubb's test for outliers in blank population		
	^{239}Pu	^{240}Pu
$\bar{Y}$	1.97	0.33
sd	3.88	0.46
G_{calc}	2.03	1.78
$G_{tab\ 0.01\ CI}$	1.94	1.75

Appendix K

The gamma spectrum obtained from measurement of Sellafield K2 25-30 cm shows the two activity peaks for ^{241}Am and ^{137}Cs (from the left).
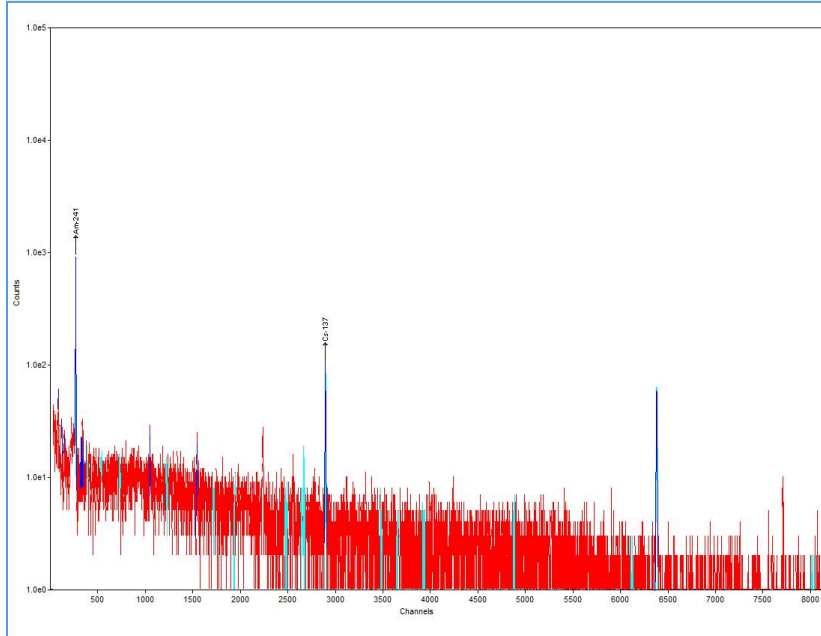
Gamma spectrum obtained from measurement of Sellafield K2 25-30 cm.

The alpha spectrum obtained from measurements of SRS A9 6-7 cm shows the 3 characteristic activity peaks for ^{242}Pu, $^{239+240}$Pu and ^{238}Pu at 4902 keV, 5168 keV and 5499 keV, respectively.
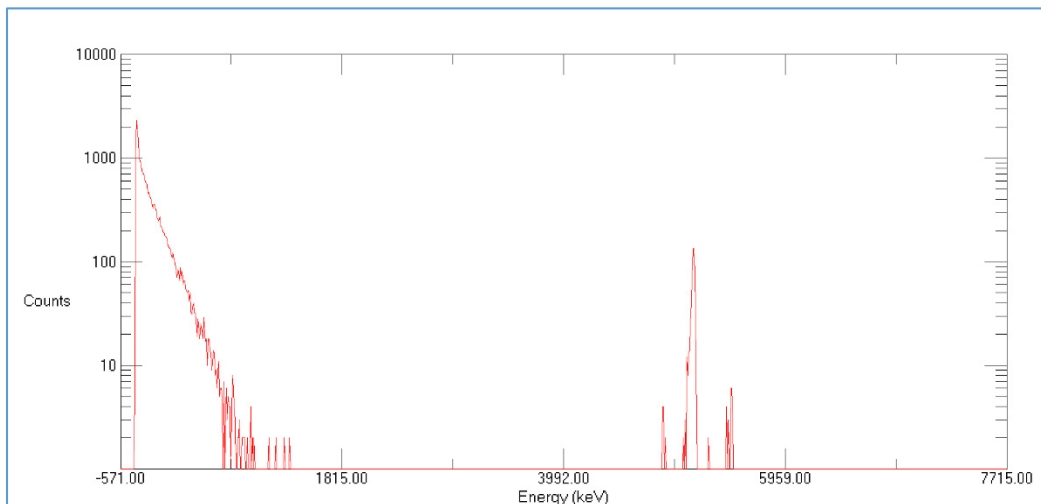
Alpha spectrum obtained from measurements of SRS A9 6-7 cm.

Appendix L

Results from calculations of Pu isotope ratios are shown below. The CPS values are adjusted for background.

$^{240}Pu/^{239}Pu$ isotope ratios for SRS A9 and Sellafield K2.

| | ^{239}Pu | | ^{240}Pu | | $^{240}Pu/^{239}Pu$ isotope | |
Sample	CPS	sigma	CPS	sigma	ratio	sigma
SRS A9 0-1	23.965	2.514	2.793	0.703	0.117	0.032
SRS A9 1-2	26.431	1.313	2.789	0.322	0.106	0.013
SRS A9 2-3	20.787	0.977	2.035	0.502	0.098	0.025
SRS A9 4-5	354.261	6.931	40.081	2.180	0.113	0.007
SRS A9 5-6	816.375	11.720	88.301	3.756	0.108	0.005
SRS A9 6-7	895.447	12.713	112.103	7.881	0.125	0.009
SRS A9 7-8	632.185	4.741	61.125	1.897	0.097	0.003
SRS A9 8-9	506.533	12.016	42.835	1.701	0.085	0.004
SRS A9 9-10	412.089	9.233	35.259	1.328	0.086	0.004
SRS A9 10-11	334.439	6.023	25.591	2.177	0.077	0.007
SRS A9 11-12	390.553	7.315	28.945	2.513	0.074	0.007
SRS A9 12-13	117.853	3.628	9.391	0.824	0.080	0.007
SRS A9 13-14	50.767	2.861	3.991	1.204	0.079	0.024
SRS A9 14-15	23.165	2.038	1.747	0.278	0.075	0.014
SRS A9 15-16	9.077	1.306	0.5715	0.451	0.063	0.051
SRS A9 16-17	9.609	0.735	0.901	0.289	0.094	0.031
SRS A9 17-18	32.323	1.474	2.257	0.617	0.070	0.019
K2 0-2	3781.665	36.004	796.555	8.976	0.211	0.003
K2 2-4	3285.567	18.733	679.813	6.654	0.207	0.002
K2 4-6	2031.575	15.469	420.781	9.129	0.207	0.005
K2 6-8	3698.043	20.069	797.953	11.946	0.216	0.003
K2 8-10	3904.033	26.806	820.001	5.877	0.210	0.002
K2 10-15	3721.271	34.713	774.751	3.511	0.208	0.002
K2 15-20	3769.463	35.906	804.821	9.685	0.214	0.003
K2 20-25	4147.967	15.464	916.029	12.161	0.221	0.003
K2 25-30	5968.341	47.238	1323.421	13.695	0.222	0.003